NACA RM A50G06

UNCLASSIFIED

NACA

RESEARCH MEMORANDUM

LOW-SPEED INVESTIGATION OF A 0.16-SCALE MODEL OF THE X-3 AIRPLANE - LONGITUDINAL CHARACTERISTICS

By Noel K. Delany and Nora-Lee F. Hayter

Ames Aeronautical Laboratory
Moffett Field, Calif.

NATIONAL ADVISORY COMMITTEE FOR AERONAUTICS

WASHINGTON
September 8, 1950

UNCLASSIFIED

NATIONAL ADVISORY COMMITTEE FOR AERONAUTICS

RESEARCH MEMORANDUM

LOW-SPEED INVESTIGATION OF A 0.16-SCALE MODEL OF THE X-3 AIRPLANE – LONGITUDINAL CHARACTERISTICS

By Noel K. Delany and Nora-Lee F. Hayter

SUMMARY

A wind-tunnel investigation has been made of the low-speed static longitudinal characteristics of a model of the X-3 airplane with the wing flaps neutral and deflected. The X-3 airplane utilizes a wing having an aspect ratio of 3.01, a 4.5-percent-thick hexagonal section, and a taper ratio of 0.4. The wing was equipped with plain leading-edge flaps and split trailing-edge flaps. The tests were conducted at a Mach number of approximately 0.20 and a Reynolds number of approximately 2,000,000.

The data indicate that the airplane, without the jettisonable-nose fins or the original main-gear doors, will be longitudinally stable from zero lift coefficient to the stall with the flaps either neutral or fully deflected and that the horizontal tail will be sufficiently effective to balance the airplane at the stall. The jettisonable nose fins and the original main-landing-gear doors both decreased the static longitudinal stability. Other main-gear doors were developed that were not detrimental to the static longitudinal stability of the airplane.

The fuselage had a large effect on the static longitudinal stability of the model. The pitching moment of the isolated fuselage was a large portion of the pitching moment of the complete model, and near the stall the downwash from the fuselage had a pronounced destabilizing effect.

It was found that the best leading-edge-flap deflection was 30° and that with the leading-edge flap deflected 30° the best trailing-edge-flap deflection was 50°.

INTRODUCTION

A supersonic research airplane such as the X-3, which incorporates such design features as a thin, low-aspect-ratio wing and a large fuselage, would be expected to present stability problems in low-speed flight, landing, and take-off. Preliminary investigation of a 0.16-scale model of the X-3 airplane at low and high subsonic Mach numbers in the Ames 16-foot high-speed wind tunnel (reference 1) indicated the airplane possessed undesirable longitudinal characteristics and that detailed testing of the model at low subsonic speeds was desirable.

An investigation was therefore undertaken in the Ames 7- by 10-foot wind tunnel to determine the cause of the undesirable low-speed characteristics and, if possible, to improve them without compromising the high-speed characteristics of the airplane. Tests were also conducted to determine the complete longitudinal characteristics of the X-3 airplane in low-speed flight. The results of these tests are presented in this report.

COEFFICIENTS AND SYMBOLS

All forces and moments were computed with respect to mutually perpendicular axes passing through the center of gravity. The longitudinal axis was parallel to the free stream and coincided with the fuselage reference line for an angle of attack of 0°. The lateral axis was parallel to the wing 75-percent-chord line. The force and moment center was on the fuselage reference line and 0.15 of the wing mean aerodynamic chord behind the leading edge of the wing mean aerodynamic chord.

The following coefficients and symbols are used in this report:

C_D drag coefficient $\left(\frac{\text{drag}}{qS}\right)$

C_L lift coefficient $\left(\frac{\text{lift}}{qS}\right)$

C_m pitching-moment coefficient $\left(\frac{\text{pitching moment}}{qS\bar{c}}\right)$

C_{m_o} pitching-moment coefficient at zero lift

P pressure coefficient $\left(\frac{\Delta p}{q}\right)$

ΔC_D increment of drag coefficient

ΔC_L increment of lift coefficient

ΔC_m increment of pitching-moment coefficient

α angle of attack of the fuselage reference line, degrees

$\Delta\alpha$ increment of angle of attack, degrees

δ_{LF} deflection of undivided leading-edge flap, positive downward, degrees

δ_{ILF} deflection of inner portion of the divided leading-edge flap, positive downward, degrees

δ_{OLF} deflection of outer portion of the divided leading-edge flap, positive downward, degrees

δ_{TF} deflection of split trailing-edge flap, positive downward, degrees

ϵ downwash angle at the horizontal tail, degrees

Δp difference in local static pressure and free-stream static pressure, pounds per square foot

q free-stream dynamic pressure $\left(\frac{1}{2}\rho V^2\right)$, pounds per square foot

q_t dynamic pressure at the horizontal tail $\left(\frac{1}{2}\rho_t {V_t}^2\right)$, pounds per square foot

ρ mass density of the air in the free stream, slugs per cubic foot

ρ_t mass density of the air at the tail, slugs per cubic foot

V free-stream velocity, feet per second

V_t stream velocity at the tail, feet per second

V_i indicated airspeed, miles per hour

V_s stalling speed, miles per hour

W/S wing loading, pounds per square foot

b wing span, feet

$\bar{c}$ mean aerodynamic chord of the wing $\left(\dfrac{\int_0^{0.5b} c^2 dy}{\int_0^{0.5b} c\ dy}\right)$, feet

S wing area, leading and trailing edges projected to fuselage center-line plane, square feet

i_t incidence of the horizontal tail measured with respect to the fuselage reference line, positive deflection with the trailing edge down, degrees

MODEL AND APPARATUS

A diagrammatic sketch of the 0.16-scale model of the X-3 airplane is shown in figure 1. Table I presents the geometric characteristics of the model and the airplane.

The wing of the model had a hexagonal section parallel to the air stream with rounded corners at 30- and 70-percent chord. It had an aspect ratio of 3.01, a thickness-to-chord ratio of 4.5 percent, and a taper ratio of 0.40. The 75-percent-chord line of the wing was straight and perpendicular to the body axis. Because of the model structure, it was not possible to test the wing of the model alone; therefore, a wing identical in plan form and section to that of the model was constructed for use in tests of an isolated wing.

The wing was normally equipped with full-span, plain, leading-edge flaps of constant chord (2 inches, parallel to the plane of symmetry) and with partial-span, split, trailing-edge flaps of 25-percent chord extending to 70 percent of the wing span. The wing was also supplied with other leading-edge flaps identical to those described above but divided at 6.25, 12.5, 25.0, or 37.5 percent of the exposed flap span measured from the fuselage, so that the inner portion of the flap could be deflected independently of the outer portion. Leading-edge-flap brackets that simulated the external flap-bracket fairings on the airplane were used on the lower surface of the wing of the model. Flap brackets were provided for deflecting the leading-edge flaps 10°, 20°, 30°, and 40° and the trailing-edge flaps 20°, 40°, 50°, and 60°. Construction of both wings was such that there was no leakage between the wings and the flaps.

The all-movable horizontal tail had a section similar to that of the wing and the 50-percent-chord line was swept back 23°. The tail incidence was varied by rotation about a line passing through the 25-percent point of the tail mean aerodynamic chord. There was no separate elevator.

The configuration referred to as the complete model consisted of the wing, the fuselage, and the tail. To this basic configuration were added nose fins, landing gear, air scoops, or canopy, as indicated.

For pilot escape at supersonic speeds the nose of the airplane, including the pilot's enclosure, was originally designed to be jettisonable.

Stabilizing fins (fig. 2) for the jettisonable nose section were tested on the model. The fins had circular-arc sections of 3-percent thickness. The fins were 120° apart with one on top of the fuselage in the plane of symmetry. This arrangement was designated as the normal position of the fins in reference 1.

The original main-gear doors are shown in figure 3(a), and the subsequent modifications to these doors are shown in figures 3(b), 3(c), 3(d), and 3(e). The nose gear and door, of which only one type was tested, are shown in figure 4.

The air scoops (fig. 5) were made with recessed faces and without ducts, so there was no internal flow. The canopy, which was also tested on the complete model, is shown in figure 6. Due to the manner in which the model was constructed, it was impossible to test the complete model with the air scoops and the canopy installed simultaneously.

Figure 7 shows the model mounted in the wind tunnel on the single support strut. Lift and drag were measured with the wind-tunnel balance system, while pitching moments were measured with a resistance-type strain gage within the model. Pressure distributions were measured by means of flush orifices arranged in chordwise rows along the upper and lower surfaces of the wing. Figure 8 shows the locations of the rows of orifices on the wing. Downwash and dynamic pressure at the tail of the model were measured with a multiple-tube rake. The locations of the rake tubes with respect to the model are shown in figure 9.

A ground plane, raised 6 inches above the tunnel floor to exclude the tunnel boundary layer, was used in determining the characteristics of the model in the presence of the ground. The wing-chord plane of the model for an angle of attack of 0° was 11.75 inches (0.28 wing span) above the ground plane and the center of gravity was 11.83 inches above the ground plane. For the other angles of attack at which the model was tested the center of gravity remained essentially at the same height above the ground plane.

CORRECTIONS TO DATA

The data have been corrected for the effects of tunnel-wall interference by the method of reference 2. The following corrections were added:

Without the ground plane

$$\Delta\alpha = 0.382\ C_L$$

$$\Delta C_D = 0.0067\ C_L{}^2$$

$$\Delta C_m = 0.0088\ C_L \quad (\Delta C_m = 0 \text{ for the data obtained with the tail off})$$

With the ground plane

$$\Delta\alpha = 0.029 \; C_L$$
$$\Delta C_D = 0.0005 \; C_L^2$$
$$\Delta C_m = 0$$

The data have not been corrected for the effects of the model-support strut. Previous investigations, however, using a similar support system and a similar model have indicated that the effect of the strut on the lift was small. Since the pitching moments were measured within the model by means of a resistance-type strain gage, the pitching-moment tares originated only from the interference between the model and the single support strut. Although drag tares were of a significant magnitude, no corrections were applied. It is believed, however, that the drag increments due to flap deflection were not greatly affected by the interference of the strut.

The single support strut used for the wing-alone tests was slightly smaller than the one used for the complete-model tests. However, the tares for the two different support struts are believed to have been of the same order of magnitude.

RESULTS AND DISCUSSION

The data obtained from tests of the 0.16-scale model of the X-3 airplane are presented in figures 10 to 41. Although some of the figures are not discussed in detail, they are considered to be of sufficient general interest for inclusion in this report. An index of the figures is presented in table II. All the test results were obtained at a Reynolds number at approximately 2×10^6.

Figures 10 to 23 present the results for the model with the flaps neutral and fully deflected. The results for the model in the presence of a ground plane (flaps neutral and fully deflected) are presented in figures 24 to 27. Figures 28 to 31 present the flap effectiveness and the effect of partial deflection of the flaps on the static longitudinal stability and on the maximum lift coefficient. The effect of nose fins, main-gear doors, vertical location of the horizontal tail, divided leading-edge flaps, pilot's canopy, and air scoops on the characteristics of the complete model are presented in figures 32 to 41.

Static Longitudinal Characteristics, Flaps Neutral

The effects of the component parts of the complete model on the lift and pitching-moment characteristics are shown in figure 10. With the wing alone, a lift coefficient at the stall[1] of 0.73 was obtained at an angle of attack of 14.5°. The addition of the fuselage reduced the stalling angle of the wing to 11.5° and the maximum lift coefficient to 0.67. The lift of the isolated fuselage was computed (fig. 10) by the use of potential theory as outlined in reference 3 for angles of attack up to 22°. Good agreement was obtained between the experimental and computed lift coefficients of the fuselage for angles of attack up to 12°. Above 12° angle of attack potential theory does not predict a large enough lift force. If the viscous effects are accounted for by the method of reference 4, the predicted lift coefficient was too great for angles of attack above 8°. The nature of the stall was changed by the addition of the fuselage (fig. 10). For the wing-fuselage combination, the lift coefficient decreased slightly when the wing stalled and then increased as the angle of attack was increased. The increase in the lift coefficient after the wing stalled was possibly due to the direct lift of the fuselage. A comparison of $dC_L/d\alpha = 0.026$ for the wing-fuselage combination after the wing stall with $dC_L/d\alpha = 0.0125$ for the fuselage alone would refute this possibility. It was found, however, that relatively small longitudinal strips along the sides of the isolated fuselage, which apparently simulated a small unstalled portion of the wing root, greatly increased the lift-curve slope of the fuselage.

The effect of Reynolds number on the lift characteristics of the model may be small, as indicated by the results of tests of a similar wing (reference 5) which were made over a Reynolds number range of 2×10^6 to 10×10^6. The minimum flight Reynolds number at sea level for the airplane with the flaps and gear retracted will be approximately 17×10^6.

Figure 10 also shows the variation of the pitching-moment coefficient with angle of attack for the wing, the fuselage, and the wing-fuselage combination. The rapid change in the slope of the pitching-moment curve, $dC_m/d\alpha$ for the wing or the wing-fuselage combination at angles of attack of 6° to 8° can be attributed to the chordwise growth of a region of separation where the flow separates at the wing leading edge and reattaches, forming a bubble. This separation is indicated by the wing pressure distributions shown in figure 11 by the region of approximately uniform minimum pressure on the upper surface for angles of attack of 4° to 11°. The region of uniform minimum pressure was relatively small at an angle of attack of 4° but rapidly extended rearward along the chord as the angle of attack was increased. The formation of the separated region was also observed at very low wind-tunnel speeds with the aid of a filament of smoke.

---

[1]Stall is herein defined as the condition where the slope of the lift curve first becomes zero at a positive angle of attack.

The results shown in figure 10 indicate that the static, longitudinal stability parameter $dC_m/d\alpha$ for the basic fuselage was 0.0088 for angles of attack up to approximately 12°. Computations, using the force distribution calculated from potential theory as outlined in reference 3, give a value of $dC_m/d\alpha = 0.0080$, which is in good agreement with the measured value.

A comparison (fig. 10) of the variation of pitching-moment coefficient with angle of attack for the wing, the fuselage, and the wing-fuselage combination indicates a stabilizing wing-fuselage interference up to an angle of attack of 12°. For angles of attack between 12° and 16° the wing-fuselage interference was destabilizing. Above an angle of attack of 16° the wing-fuselage interference was again stabilizing.

The component effects of the fuselage on the longitudinal stability of the model are shown in figure 12. The contribution of the horizontal tail to the pitching moment was computed for the wing with the tail and for the wing-fuselage combination with the tail by use of the data shown in figures 13 and 14 (downwash and loss of dynamic pressure at the hinge line of the horizontal tail) and the data of reference 6. With this pitching moment due to the tail and with the data of figure 10, figure 12 was constructed. The major effects of the fuselage on the stability of the complete model may be seen to be due to the large pitching moment of the isolated fuselage and the downwash produced by the fuselage after the wing stall. The effect of the wing-fuselage interference, previously mentioned, on the stability was of small magnitude. Previous to the wing stall, the effect of the downwash due to the fuselage was of small consequence. After the wing stall, however, the effect of the fuselage downwash was very destabilizing, as is indicated by the change in $dC_m/d\alpha$.

The lift and pitching-moment characteristics for the complete model are presented in figure 15 for several incidences of the all-movable horizontal tail. The effectiveness of the horizontal tail, as indicated by a value of dC_m/di_t of approximately −0.026, was sufficiently large to indicate that the airplane can be balanced with the center of gravity as far forward as 0.05 of the mean aerodynamic chord behind the leading edge of the mean aerodynamic chord. After the wing stall, the horizontal-tail effectiveness decreased somewhat due to the decrease in the dynamic pressure at the tail. The variation of the horizontal-tail incidence i_t with indicated airspeed for the airplane in steady, straight, unyawed flight (fig. 16) was estimated from the data for the complete model with the flaps neutral (fig. 15). These curves indicate that with the center of gravity at 5, 10, or 15 percent of the mean aerodynamic chord and with a wing loading of 100 pounds per square foot the stability will be satisfactory. The minimum indicated airspeed obtainable with the flaps and gear retracted for a wing loading of 100 pounds per square foot would be approximately 243 miles per hour for unstalled flight, as indicated by the test results.

Static Longitudinal Characteristics, Flaps Fully Deflected

The effect of the component parts of the complete model, with the leading-edge flaps deflected 30° and the trailing-edge flap deflected 50°, on the lift and pitching-moment characteristics is shown in figure 17. With the wing alone (leading-edge and trailing-edge flaps extended inward to the plane of symmetry), a maximum lift coefficient of 1.55 was obtained at an angle of attack of 19.5°. The addition of the fuselage to the wing decreased the stalling angle of the combination approximately 1.5°. Furthermore, at an angle of attack of 0°, the addition of the fuselage reduced the increment of lift coefficient developed by the split trailing-edge flap from 0.52 to 0.31.

As mentioned previously in the discussion of the longitudinal characteristics of the model with the flaps neutral, the effect of Reynolds number may be small. This is indicated by the results of tests which were made for a similar wing (reference 7) over a Reynolds number range of 3×10^6 to 10×10^6. The Reynolds number of the X-3 airplane in approach and landing will be approximately 13×10^6.

The variation of the pitching-moment coefficient with angle of attack for the wing, the fuselage, and the wing-fuselage combination is shown in figure 17. The rapid change in the slope of the pitching-moment curve $(-dC_m/d\alpha)$ for the wing-fuselage combination or for the wing alone at an angle of attack of approximately 16° is due possibly to wing-leading-edge separation. It cannot be ascertained from the available data if the separation was similar to the bubble noted with the flaps retracted. The tuft studies, however, did indicate rough flow over the center portion of both wing panels at approximately 16° angle of attack. The pressure distributions in figure 18 show that the center of pressure moved rearward rapidly at approximately 16° angle of attack. A comparison of the variation of the pitching-moment coefficient with angle of attack for the wing-fuselage combination with that calculated as a summation of the pitching moments of the wing and fuselage indicates a stabilizing wing-fuselage interference for angles of attack from 0° to 18° (wing stall). Besides the change in stability, there was a large positive C_{m_0} shift due to the removal of the center section of the trailing-edge flap to accommodate the fuselage.

The effects of the fuselage on the longitudinal stability of the model are separated in figure 19. The contribution of the horizontal tail to the wing-plus-tail curve was computed using the data of reference 6 and the data of figures 20 and 21 (downwash and loss of dynamic pressure at the hinge line of the horizontal tail). Examination of figure 19 shows that, as with flaps neutral, one of the major effects of the fuselage was due to the large pitching moment of the isolated fuselage. The wing-fuselage interference was also of a large magnitude throughout the angle-of-attack range tested. The effect of the fuselage on the changes in downwash and dynamic pressure at the tail was of relatively small importance below an angle of attack of approximately 12°. Above this angle of attack, however, the changes in downwash and in dynamic pressure due to the fuselage were of major importance (fig. 19). Reference to figure 17 shows that the lift-curve slope for the isolated fuselage started to increase at approximately this same angle of attack ($\alpha = 12^\circ$). Furthermore, figure 10 shows the agreement between the test data and potential theory is not good above an angle of attack of 12°, indicating that there was a definite change in the character of the flow over the fuselage at the higher angles of attack.

The data of figures 22 and 23 indicate that the airplane will be longitudinally stable throughout the test angle-of-attack range with the center of gravity as far aft as 15 percent of the mean aerodynamic chord behind the leading edge of the mean aerodynamic chord. The data also indicate sufficient horizontal-tail effectiveness to balance the airplane at the minimum flight speed with the center of gravity as far forward as 5 percent of the mean aerodynamic chord. With a wing loading of 100 pounds per square foot, the minimum indicated airspeed attainable would be approximately 172 miles per hour. A comparison of the variation of incidence of the horizontal tail with indicated airspeed for the flaps neutral (fig. 16) and for the flaps fully deflected (fig. 23) indicates a rather large change in the horizontal-tail incidence to balance the airplane as the flaps are deflected.

Static Longitudinal Characteristics in the Presence of a Ground Plane

For the tests with the model in the presence of the ground plane the nose gear, the nose-gear door, and the main gear were installed on the model to simulate take-off with the flaps neutral and to simulate landing with the flaps fully deflected. Figures 24 to 27 present the lift and static, longitudinal stability characteristics of the model with the flaps neutral and fully deflected.

With the flaps neutral, a comparison of the data of figures 24 and 15 shows that the proximity of the model to the ground plane increased the maximum lift coefficient and the static longitudinal stability. With the center of gravity 15 percent of the mean aerodynamic chord behind the leading edge of the mean aerodynamic chord, the maximum lift coefficient for balance was increased from 0.66 to 0.70. With a wing loading of 100 pounds per square foot, however, this would amount to a decrease by only 7 miles per hour of the minimum attainable indicated airspeed. At approximately 1.2 times the stalling speed ($C_L = 0.5$), the nearness of the model to the ground plane changed the value of dC_m/dC_L from −0.155 to −0.238 (center of gravity at 15 percent of the mean aerodynamic chord). With the most forward center-of-gravity location anticipated (5 percent of the mean aerodynamic chord), the horizontal tail was sufficiently effective to balance the model at the stall.

With the flaps fully deflected, the proximity of the model to the ground plane decreased the angle of attack at which the wing stalled from 18.5° to 14.8° with a consequent decrease in the lift coefficient at the stall of 0.06 (figs. 22 and 26). At approximately 1.2 times the stalling speed and with a wing loading of 100 pounds per square foot, the static longitudinal stability was increased from $dC_m/dC_L = -0.081$ to -0.296 (center of gravity at 15 percent mean aerodynamic chord). As was the case with the flaps neutral, the results indicate that the horizontal tail is sufficiently effective to balance the airplane at the stall with the most forward center-of-gravity location (5 percent mean aerodynamic chord behind the leading edge of the mean aerodynamic chord).

Static Longitudinal Characteristics, Flaps Partially Deflected

The variation of the lift coefficient at the stall with leading- and trailing-edge-flap deflections is shown in figure 28. Of the four leading-edge-flap deflections tested ($\delta_{LE} = 10^\circ$, 20°, 30°, and 40°), the 30° deflection produced the highest lift coefficients for trailing-edge-flap deflections less than 50°. Two-dimensional test data from reference 8 for a similar, thin, sharp-edged airfoil have also indicated that the maximum beneficial leading-edge-flap deflection was about 30°. With the leading-edge flap deflected 30°, a deflection of the trailing-edge split flap of 50° produced the highest lift coefficient.

Figure 29 shows the variation of drag coefficient with lift coefficient for various leading- and trailing-edge-flap deflections. As previously mentioned, no corrections have been applied to the data for the effects of the model support. The drag and interference of the model support changed the magnitudes of the drag coefficients, but it is believed that the drag increments and the shapes of the curves were not altered. The envelope of the lift-drag curves (fig. 29) therefore would indicate the flap deflection for minimum drag for a given lift coefficient. To follow the envelope curve for lift coefficients of 0 to approximately 0.8, the leading-edge flap should be deflected from 0° to 30° so that the flap deflection varies approximately linearly with lift coefficient. To follow the envelope curve for lift coefficients of 0.8 to the stall ($C_L = 1.4$), the leading-edge-flap deflection should remain constant at 30° and the trailing-edge flap should be deflected from 0° to 50° so that the trailing-edge-flap deflection varies linearly with the lift coefficient.

The effect of partial deflection of the flaps on the static longitudinal stability of the model is shown in figure 30(a). As the leading-edge-flap deflection was increased the stability decreased. With deflections of the leading-edge flap of 0° or 10° the stability was satisfactory, but with a deflection of 20° the data indicate instability prior to the stall. As the deflection was further increased to 30° the degree of instability remained about the same, but the unstable range was extended. For deflections of the leading-edge flap of 20° and 30°, the stability began to decrease markedly for lift coefficients above approximately 0.6.

The decrease in static longitudinal stability that occurred with leading-edge-flap deflection can be attributed mainly to the change in the tail-off stability (fig. 30(b)) and to an increase in the rate of change of downwash with angle of attack. This change in the stability of the model, with the tail off, was due to the delay of the leading-edge separation by the leading-edge flap. The increase in $d\epsilon/d\alpha$ may have been due to the effect of the leading-edge flap on the fuselage downwash since the decrease in stability began at approximately the angle of attack at which the lift-curve slope of the isolated fuselage (fig. 10) began to increase. Deflection of the trailing-edge flap in conjunction with the leading-edge flap had a beneficial effect on the stability and the lift for all flap configurations (fig. 31).

Effect of Miscellaneous Changes of the Model on the Longitudinal Characteristics

Nose fins.- The airplane as originally designed was to be equipped with a jettisonable nose section for pilot escape. Three fins were attached to the nose to stabilize this section in a free fall after separation from the rest of the airplane. Figure 32 presents the results of the tests with the nose fins. These results indicate that the nose fins caused large destabilizing pitching moments, due mainly to the direct lift forces produced by the nose fins. Consequently, further tests with the nose fins were abandoned early in the investigation.

Main-landing-gear doors.- The effects of several types and sizes of main-landing-gear doors are shown in figure 33. The major effect of the landing-gear doors was similar to that of the nose fins in that the horizontally projected area of the main-gear doors contributed lift forces ahead of the center of gravity, causing a destabilizing pitching moment. Removal of the original main-landing-gear doors increased the static longitudinal stability dC_m/dC_L by approximately -0.05. Other main-landing-gear doors (main-gear-door configurations 3 and 4) were developed that were not detrimental to the static longitudinal stability.

Vertical location of horizontal tail.- Figure 34 shows the effect of varying the vertical location of the horizontal tail. (See table I for the height of the tail above the wing-chord plane.) With the flaps neutral (fig. 34(a)), a considerable increase in the static longitudinal stability was obtained by raising the horizontal tail from 0.587 to 1.307 feet (model scale) above the wing-chord plane. With the wing flaps fully deflected (fig. 34(b)), a similar increase in the static longitudinal stability was obtained at the lower lift coefficients. However, above a lift coefficient of 1.1 the vertical location of the horizontal tail had a negligible effect on the stability.

Modified leading-edge flaps.— Tests were made with the leading-edge flap modified so that the inner portion of the flap could be deflected differentially with respect to the outer portion. The results of these tests are presented in figures 35 to 39. It was found that by deflecting only the outer 89.5 to 94 percent of the exposed leading-edge flap 30° the maximum lift coefficient could be significantly increased without any deleterious effect on the static longitudinal stability. This increase in the maximum lift coefficient might be explained by the action of vortices being shed at the break in the flap. The vortices possibly re-energized the wing boundary layer and kept the flow separation from spreading rapidly, thereby allowing the angle of attack to be increased several degrees more before the wing stalled.

Canopy and scoops.— Figures 40 and 41 present the results obtained with the canopy and scoops added individually to the complete model. Neither the canopy nor the scoops materially affected the variation of lift coefficient with angle of attack with flaps neutral or fully deflected. There was, however, a small increase in the maximum lift coefficient, with the flaps fully deflected, due to the addition of either the canopy or the scoops. The major effect of the canopy on the variation of the pitching-moment coefficient with lift coefficient was a small C_{m_0} shift with the flaps neutral. The scoops caused a C_{m_0} shift and a slight decrease in the stability with the flaps neutral or fully deflected.

CONCLUSIONS

The following conclusions can be drawn from the data obtained during the low-speed tests of the 0.16-scale model of the X-3 airplane conducted in the Ames 7- by 10-foot wind tunnels:

1. The airplane without the nose fins or the original gear doors will be longitudinally stable from zero lift to the stall with leading-edge and trailing-edge flaps fully deflected or neutral with the center of gravity at 0.15 of the wing mean aerodynamic chord.

2. The horizontal-tail effectiveness in flight or in the presence of the ground will be sufficient to balance the airplane at the stall with the flaps neutral or fully deflected.

3. Removal of the main-landing-gear doors increased the static longitudinal stability with the flaps fully deflected.

4. The destabilizing moment of the isolated fuselage was a large portion of the pitching moment of the complete model.

5. Near the stall the changes in the downwash at the tail, due to the fuselage, had a pronounced effect on the static longitudinal stability.

6. The large destabilizing effect of the fins on the jettisonable nose made their use impractical.

7. The best leading-edge-flap deflection was found to be approximately 30°. It was also found that with 30° deflection of the leading-edge flap the optimum deflection of the trailing-edge split flap was approximately 50°.

8. Deflection of only the outer 88 to 91 percent of the leading-edge flap was found to improve the maximum lift coefficient without any detrimental effect on the static longitudinal stability.

Ames Aeronautical Laboratory,
National Advisory Committee for Aeronautics,
Moffett Field, California.

REFERENCES

1. Hamilton, William T., and Cleary, Joseph W.: Wind-Tunnel Tests of a 0.16-Scale Model of the X-3 Airplane at High Subsonic Speeds. - Stability and Control Characteristics. NACA RM A50A03, 1950.

2. Swanson, Robert S., and Schuldenfrei, Marvin J.: Jet-Boundary Corrections to the Downwash Behind Powered Models in Rectangular Wind Tunnels with Numerical Values for 7- by 10-Foot Closed Wind Tunnels. NACA ARR, 1942.

3. Laitone, E. V.: The Linearized Subsonic and Supersonic Flow About Inclined Slender Bodies of Revolution. Jour. Aero. Sci., vol. 14, no. 11, Nov. 1947, pp. 631-642.

4. Allen, Julian H.: Estimation of the Forces and Moments Acting on Inclined Bodies of Revolution of High Fineness Ratio. NACA RM A9I26, 1949.

5. Johnson, Ben H., Jr.: Investigation of a Thin Wing of Aspect Ratio 4 in the Ames 12-Foot Pressure Wind Tunnel. I - Characteristics of a Plain Wing. NACA RM A8D07, 1948.

6. DeYoung, John: Theoretical Additional Span Loading Characteristics of Wings With Arbitrary Sweep, Aspect Ratio, and Taper Ratio. NACA TN 1491, 1947.

7. Johnson, Ben H., Jr., and Bandettini, Angelo: Investigation of a Thin Wing of Aspect Ratio 4 in the Ames 12-Foot Pressure Wind Tunnel. II – The Effect of Constant-Chord Leading- and Trailing-Edge Flaps on the Low-Speed Characteristics of the Wing. NACA RM A8F15, 1948.

8. Rose, Leonard M., and Altman, John M.: Low-Speed Experimental Investigation of a Thin, Faired, Double-Wedge Airfoil With Nose and Trailing-Edge Flaps. NACA TN 1934, 1949.

TABLE I.– GEOMETRIC CHARACTERISTICS OF THE MODEL AND AIRPLANE

	Model	Airplane
Wing		
Area, square feet	4.091	159.81
Aspect ratio	3.01	3.01
Taper ratio	0.4	0.4
Span, feet	3.507	21.93
Mean aerodynamic chord, feet	1.238	7.74
Root chord, feet	1.667	10.42
Tip chord, feet	0.667	4.17
Percent thickness	4.5	4.5
Dihedral, degrees	0	0
Incidence, degrees	0	0
Sweepback (75–percent–chord line), degrees	0	0
Distance of wing–chord plane below fuselage reference plane, feet	0.078	0.487
Leading–edge flaps		
Type	Plain	Plain
Wing station at inner end, feet	0.420	2.625
Wing station at outer end, feet	1.753	10.965
Chord, feet	0.167	1.042
Maximum deflection, degrees	40	40
Trailing–edge flaps		
Type	Split	Split
Wing station at inner end, feet	0.407	2.541
Wing station at outer end, feet	1.226	7.661
Percent chord	25.0	25.0
Maximum deflection, degrees	60	60
Ailerons		
Type	Plain	Plain
Wing station at inner end, feet	1.228	7.672
Wing station at outer end, feet	1.753	10.965
Percent chord	5.0	25.0
Deflection, degrees	±15	±15

TABLE I.— CONTINUED

	Model	Airplane
Horizontal tail		
Area, square feet	0.794	31.01
Aspect ratio	3.01	3.01
Taper ratio	0.4	0.4
Span, feet	1.547	9.667
Root chord, feet	0.725	4.533
Tip chord, feet	0.293	1.833
Sweepback of 50-percent-chord line, degrees	23	23
Incidence (variable), degrees	10 to −19	10 to −30
Mean aerodynamic chord of the exposed area, feet	0.521	3.256
Exposed area, square feet	0.701	27.383
Hinge line, percent of M.A.C. of exposed area	25	25
Tail length (from 15-percent wing M.A.C. to horizontal-tail hinge line), feet	3.375	21.095
Height above fuselage reference line		
Normal tail location, feet	0.587	3.667
Intermediate tail location, feet	0.947	— — —
High tail location, feet	1.307	— — —
Vertical tail		
Area, square feet	0.678	26.50
Aspect ratio	1.32	1.32
Taper ratio	0.25	0.25
Span, feet	0.947	5.917
Root chord, feet	1.147	7.167
Tip chord, feet	0.287	1.792
Height of root chord above fuselage reference line, feet	0.688	4.302
Sweepback of 90-percent-chord line, degrees	0	0
Mean aerodynamic chord, feet	0.803	5.017
Tail length (from 15-percent wing M.A.C. to 25-percent vertical tail M.A.C.), feet	3.411	21.316
Rudder		
Span, feet	0.705	4.406
Tip chord, feet	0.176	1.098
Root chord, feet	0.238	1.488

NACA

TABLE I.– CONCLUDED

	Model	Airplane
Rudder		
Deflection, degrees	± 20	± 20
Hinge line normal to fuselage reference line	---	---
Jettisonable–nose fins		
Area of each fin, square feet	0.084	3.30
Aspect ratio	0.75	0.75
Taper ratio	0.25	0.25
Span, feet	0.253	1.583
Root chord, feet	0.533	3.333
Tip chord, feet	0.133	.833
Mean aerodynamic chord, feet	0.373	2.333
Sweepback (90–percent–chord line), degrees	0	0
Horizontal distance of the 25 percent M.A.C., feet	0.550	3.437
Assumed wing loading, pounds per square foot	---	100

NACA

TABLE II.– FIGURE INDEX

Model configuration	Tail i_t	Flap δ_{LF}	Flap δ_{ILF}	Flap δ_{OLF}	Flap δ_{TF}	Figure number C_L–α	C_m–α	C_m–C_L	C_D–C_L	$\frac{\Delta p}{q}$	ϵ	$1-\frac{q_t}{q}$	i_T–V_i	$C_{L_{max}}$
Complete model less tail	–	0	–	–	0	10	10	–	29	–	14	14	–	–
	–	0	–	–	0	15	–	15	–	–	–	–	–	–
	–	0	–	–	0	30b	–	30b	–	–	–	–	–	–
	–	0	–	–	0	34a	–	34a	–	–	–	–	–	–
	–	30	–	–	50	17	17	–	29	–	21	21	–	–
	–	30	–	–	50	22	–	22	–	–	–	–	–	–
	–	30	–	–	50	31b	–	31b	–	–	–	–	–	–
	–	30	–	–	50	34b	–	34b	–	–	–	–	–	–
	–	0	–	–	Var.	–	–	–	–	–	–	–	–	28
	–	10	–	–	Var.	–	–	–	–	–	–	–	–	28
	–	20	–	–	Var.	–	–	–	–	–	–	–	–	28
	–	30	–	–	Var.	–	–	–	–	–	–	–	–	28
	–	40	–	–	Var.	–	–	–	–	–	–	–	–	28
	–	10	–	–	0	30b	–	30b	29	–	–	–	–	–
	–	20	–	–	0	30b	–	30b	29	–	–	–	–	–
	–	30	–	–	0	30b	–	30b	29	–	–	–	–	–
	–	40	–	–	0	–	–	–	29	–	–	–	–	–
	–	30	–	–	40	–	–	–	29	–	–	–	–	–
	–	30	–	–	60	–	–	–	29	–	–	–	–	–
	–	0	–	–	50	31b	–	31b	–	–	–	–	–	–
	–	10	–	–	20	31b	–	31b	–	–	–	–	–	–
	–	20	–	–	30	31b	–	31b	–	–	–	–	–	–

TABLE II.— CONTINUED

Model configuration	Tail i_t	Flap δ_{LF}	δ_{ILF}	δ_{OLF}	δ_{TF}	Figure number C_L–α	C_m–α	C_m–C_L	C_D–C_L	$\frac{\Delta p}{q}$	ϵ	$1-\frac{q_t}{q}$	i_T–V_i	$C_{L_{max}}$
Complete model	0	0	–	–	0	10	10	–	–	11	–	–	–	–
	0	0	–	–	0	15	12	15	–	–	–	–	–	–
	–5	0	–	–	0	15	–	15	–	–	–	–	–	–
	–5	0	–	–	0	15	–	15	–	–	–	–	–	–
	Var.	0	–	–	0	–	–	–	–	–	–	–	16	–
	–	30	–	–	50	17	17	–	–	18	–	–	–	–
	–5	30	–	–	50	–	19	–	–	–	–	–	–	–
	0	30	–	–	50	22	–	22	–	–	–	–	–	–
	–5	30	–	–	50	22	–	22	–	–	–	–	–	–
	–10	30	–	–	50	22	–	22	–	–	–	–	–	–
	Var.	30	–	–	50	–	–	–	–	–	–	–	23	–
	–5	0	–	–	0	30a	–	30a	–	–	–	–	–	–
	–5	10	–	–	0	30a	–	30a	–	–	–	–	–	–
	–5	20	–	–	0	30a	–	30a	–	–	–	–	–	–
	–5	30	–	–	0	30a	–	30a	–	–	–	–	–	–
	–5	0	–	–	50	31a	–	31a	–	–	–	–	–	–
	–5	10	–	–	20	31a	–	31a	–	–	–	–	–	–
	–5	20	–	–	30	31a	–	31a	–	–	–	–	–	–
	–5	30	–	–	50	31a	–	31a	–	–	–	–	–	–
	0	–	0	30	50	35a	–	36a	–	–	–	–	–	37
	0	–	10	30	50	35b	–	36b	–	–	–	–	–	37
	0	–	20	30	50	35c	–	36c	–	–	–	–	–	37
	0	–	30	30	50	35d	–	36d	–	–	–	–	–	37

NACA

TABLE II.– CONTINUED

Model configuration	Tail i_t	Flap δ_{LF}	Flap δ_{ILF}	Flap δ_{OLF}	Flap δ_{TF}	Figure number C_L-α	Figure number C_m-α	Figure number C_m-C_L	Figure number C_D-C_L	Figure number $\frac{\Delta p}{q}$	Figure number ϵ	Figure number $1-\frac{q_t}{q}$	Figure number i_T-V_i	Figure number $C_{L_{max}}$
0.0625	0	–	0	30	50	38	–	38	–	–	–	–	–	–
	–5	–	0	30	50	38	–	38	–	–	–	–	–	–
	–10	–	0	30	50	38	–	38	–	–	–	–	–	–
0.125	0	–	0	30	50	39	–	39	–	–	–	–	–	–
	–5	–	0	30	50	39	–	39	–	–	–	–	–	–
	–10	–	0	30	50	39	–	39	–	–	–	–	–	–
Complete model in the presence of the ground	0	0	–	–	0	24	–	24	–	–	–	–	–	–
	–5	0	–	–	0	24	–	24	–	–	–	–	–	–
	–10	0	–	–	0	24	–	24	–	–	–	–	–	–
	Var.	0	–	–	0	–	–	–	–	–	–	–	25	–
	0	30	–	–	50	26	–	26	–	–	–	–	–	–
	–5	30	–	–	50	26	–	26	–	–	–	–	–	–
	–10	30	–	–	50	26	–	26	–	–	–	–	–	–
	–15	30	–	–	50	26	–	26	–	–	–	–	–	–
	–19	30	–	–	50	26	–	26	–	–	–	–	–	–
	Var.	30	–	–	50	–	–	–	–	–	–	–	27	–
Complete model less tail in the presence of the ground	–	0	–	–	0	24	–	24	–	–	–	–	–	–
	–	30	–	–	50	26	–	26	–	–	–	–	–	–

NACA

TABLE II.– CONCLUDED

Model configuration	Tail i_t	Flap δ_{LF}	Flap δ_{ILF}	Flap δ_{OLF}	Flap δ_{TF}	Figure number C_L–α	C_m–α	C_m–C_L	C_D–C_L	$\frac{\Delta p}{q}$	ϵ	$1-\frac{q_t}{q}$	i_T–V_i	$C_{L_{max}}$
Complete model with nose fins	0 –5	30 30	– –	– –	50 50	32a 32b	– –	32a 32b	– –	– –	– –	– –	– –	– –
Complete model with main gear doors	–5	30	–	–	50	33	–	33	–	–	–	–	–	–
Complete model with variable tail height	0 –5	0 30	– –	– –	0 50	34a 34b	– –	34a 34b	– –	– –	– –	– –	– –	– –
Complete model with canopy	0 –5	0 30	– –	– –	0 50	40a 40b	– –	40a 40b	– –	– –	– –	– –	– –	– –
Complete model with air scoops	0 –5	0 30	– –	– –	0 50	41a 41b	– –	41a 41b	– –	– –	– –	– –	– –	– –
Wing	– –	0 30	– –	– –	0 50	10 17	10 17	– –	– –	– –	13 20	13 20	– –	– –
Fuselage	– –	– –	– –	– –	– –	10 17	10 17	– –	– –	– –	– –	– –	– –	– –

NACA

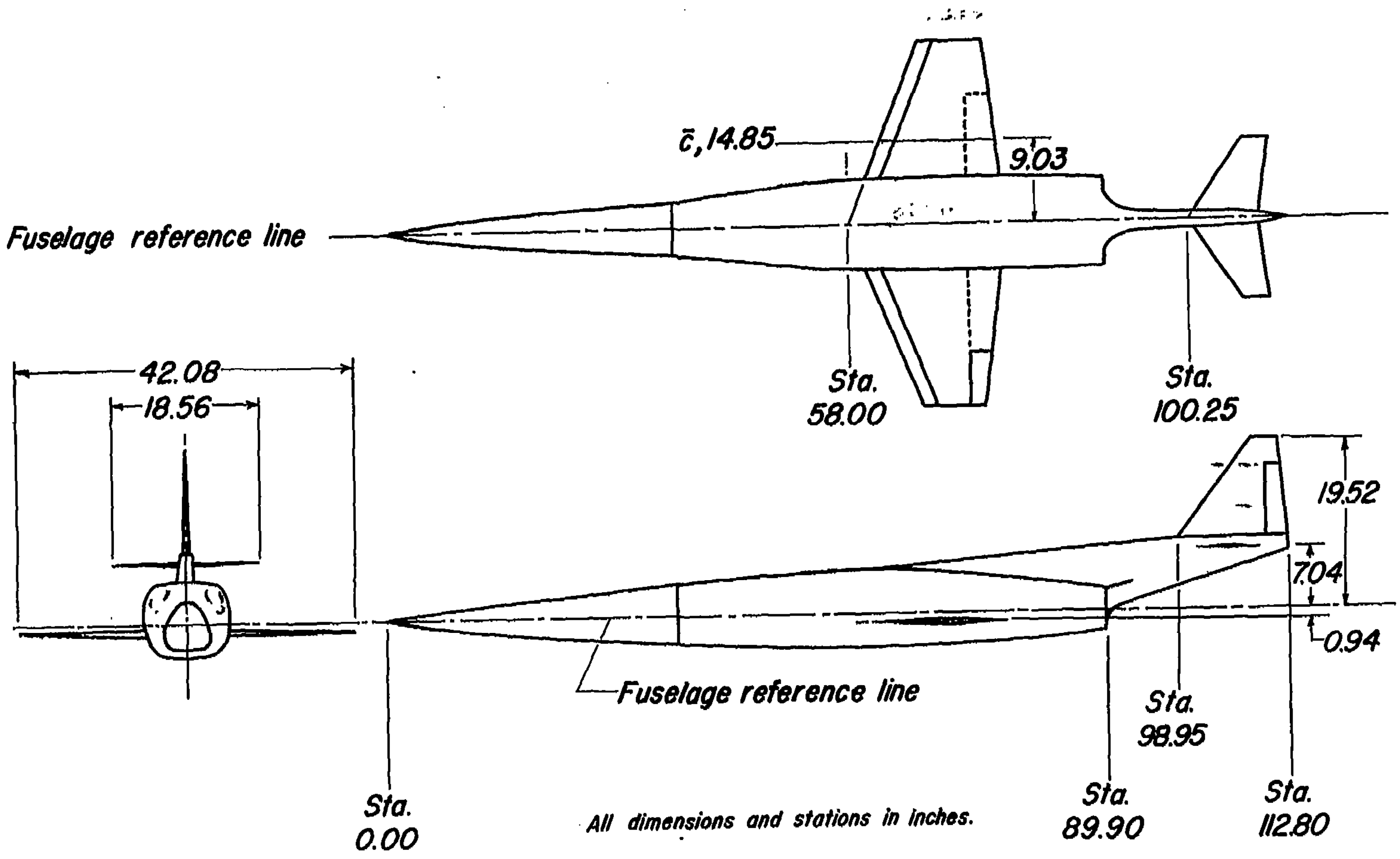

Figure 1.- Diagrammatic sketch of the model.

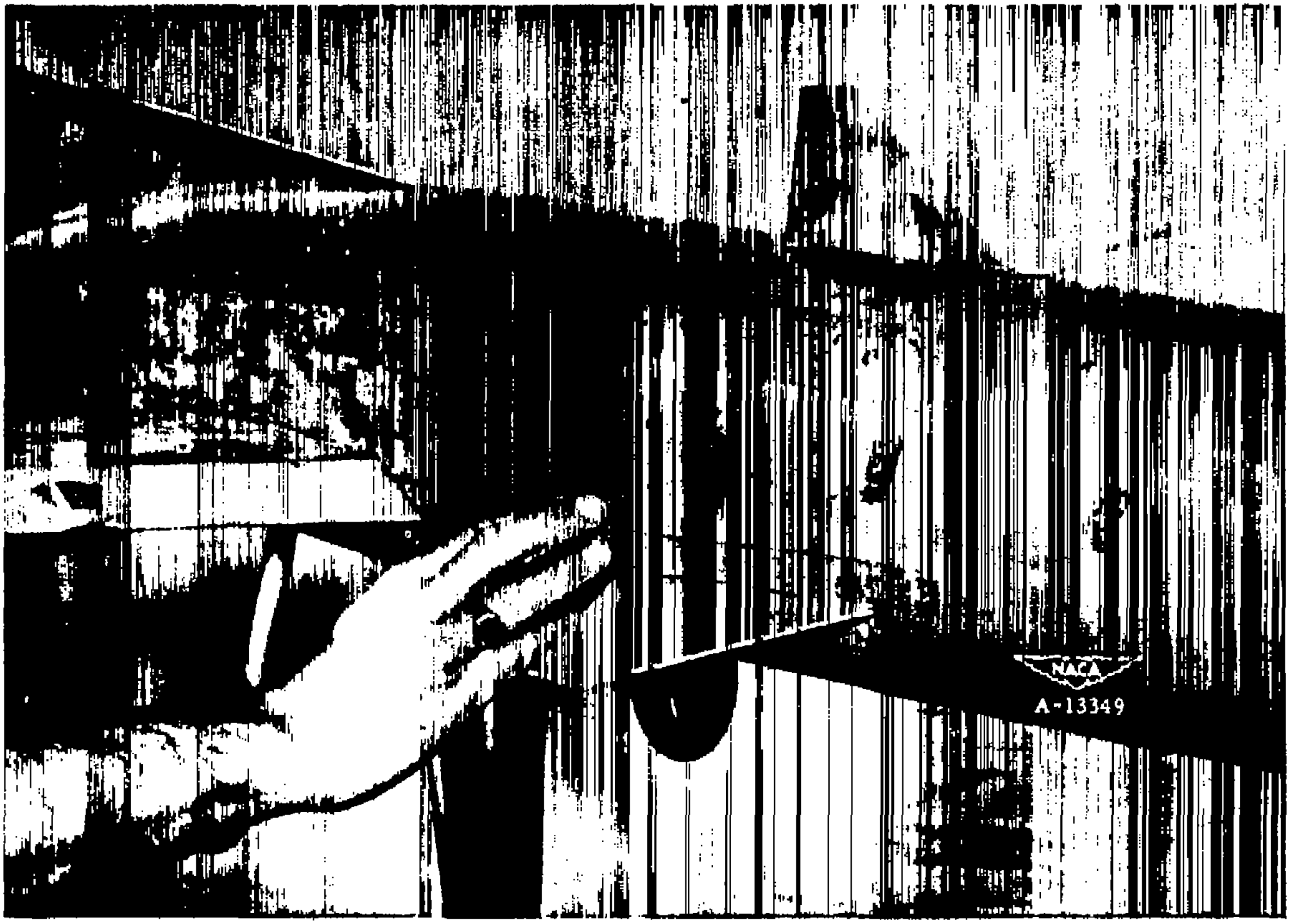

Figure 2.— Detail of the nose fins.

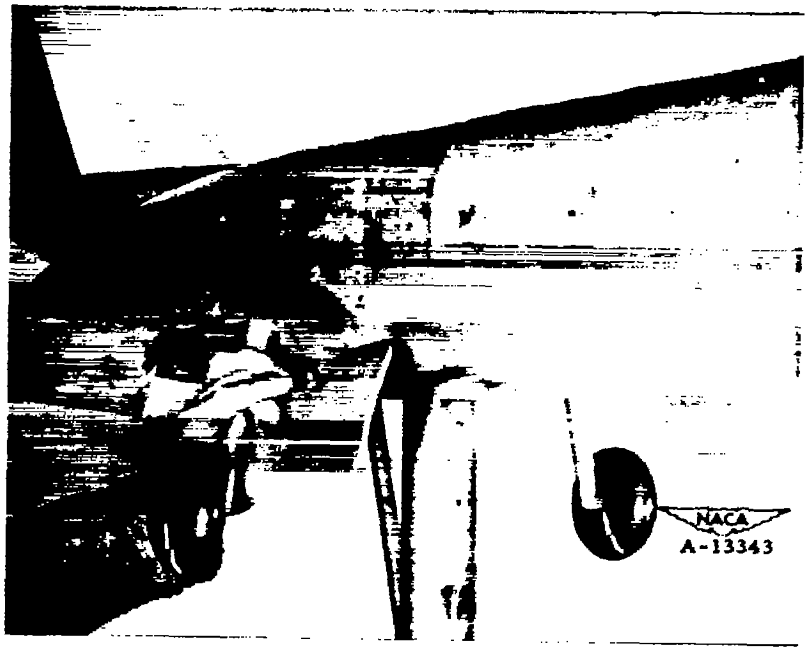

(a) Configuration 1.

(b) Configuration 2.

Figure 3.— Detail of the various main-gear-door configurations.

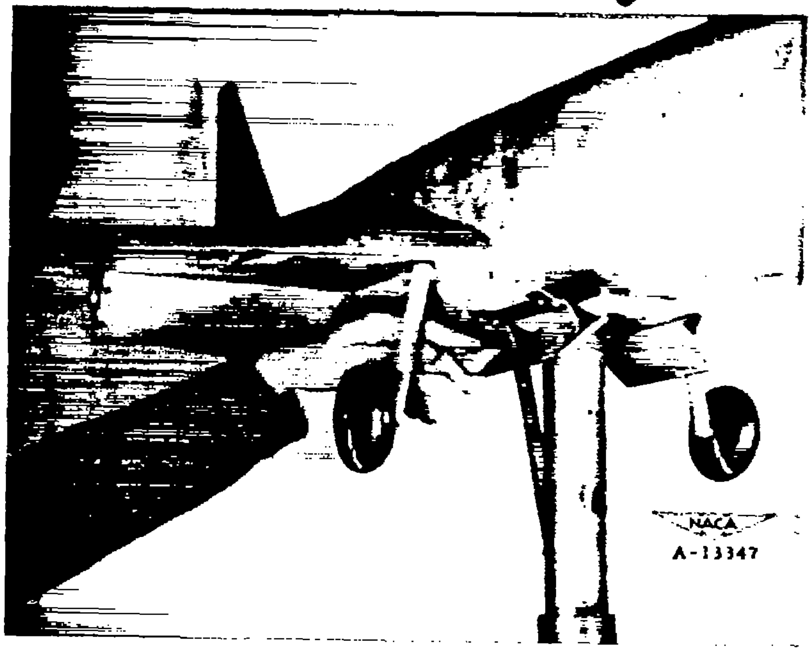

(c) Configuration 3.

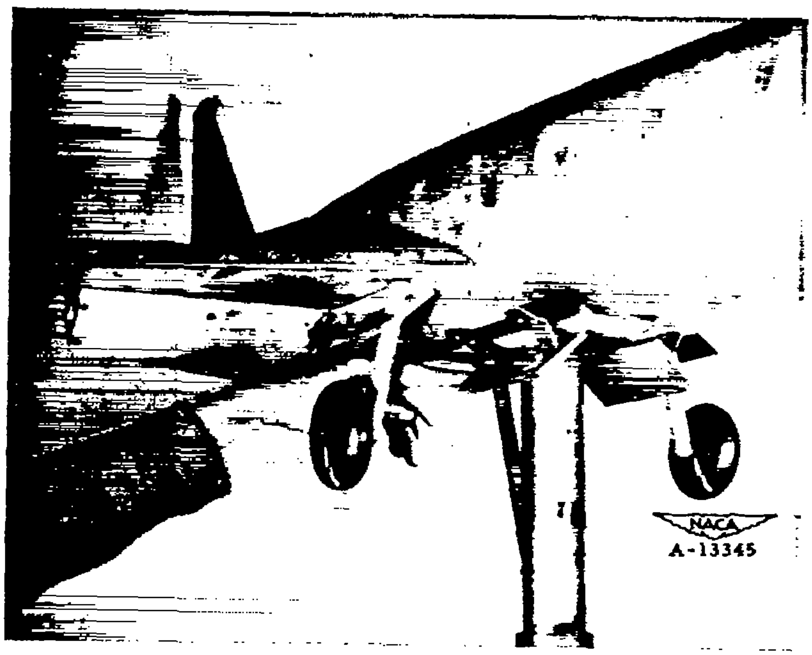

(d) Configuration 4.

Figure 3.— Continued.

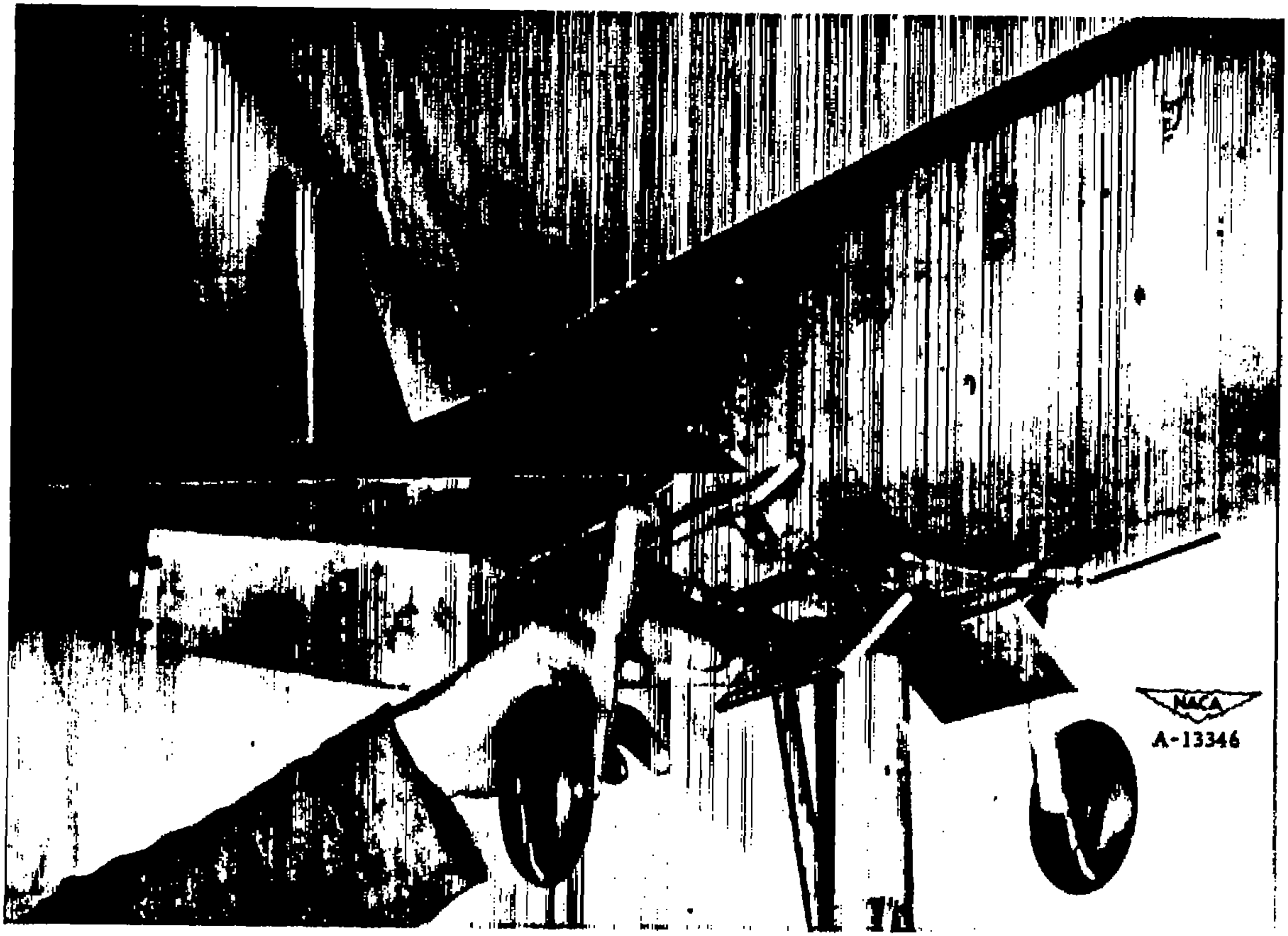

(e) Configuration 5.

Figure 3.– Concluded.

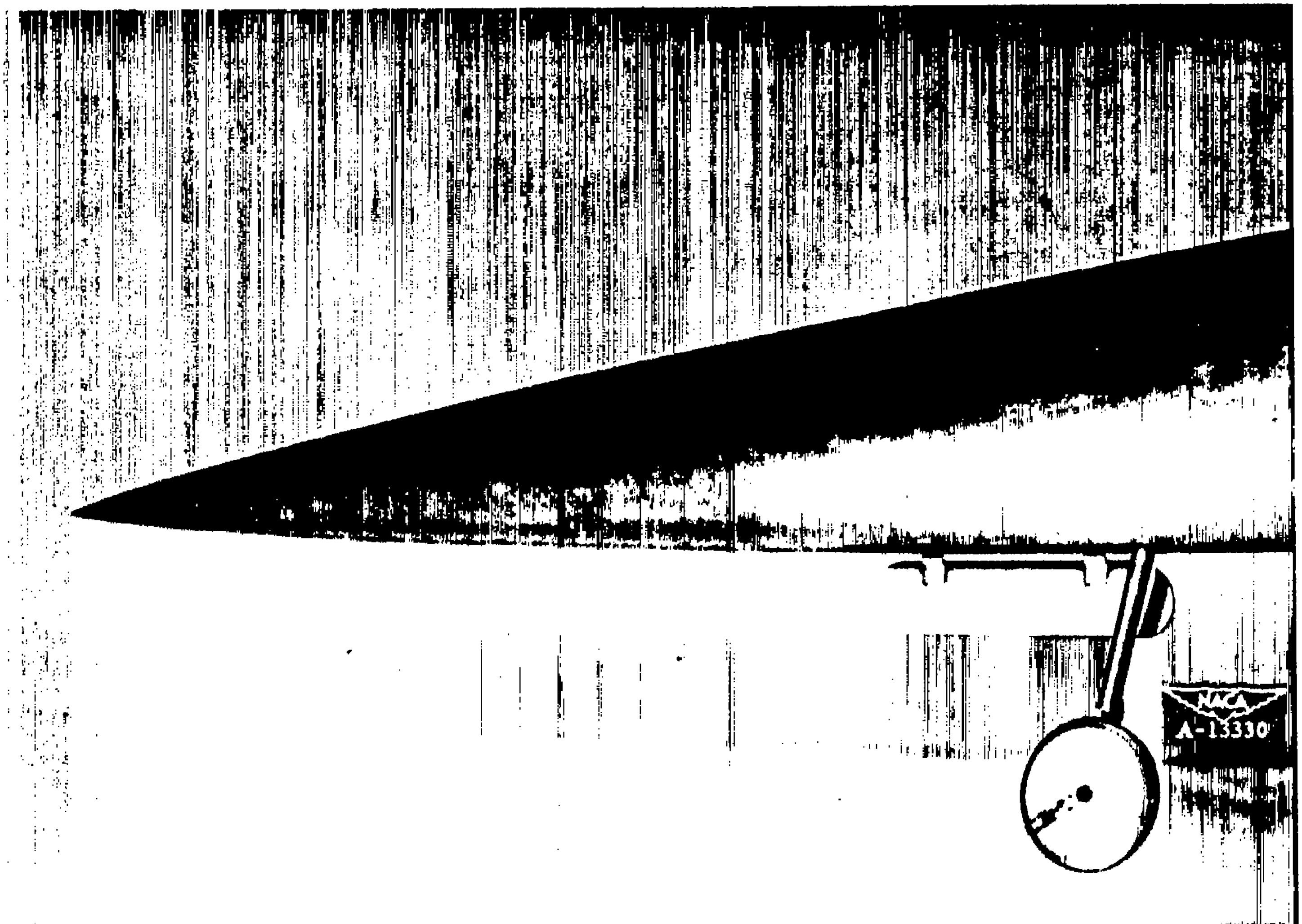

Figure 4.— Detail of the nose gear and door.

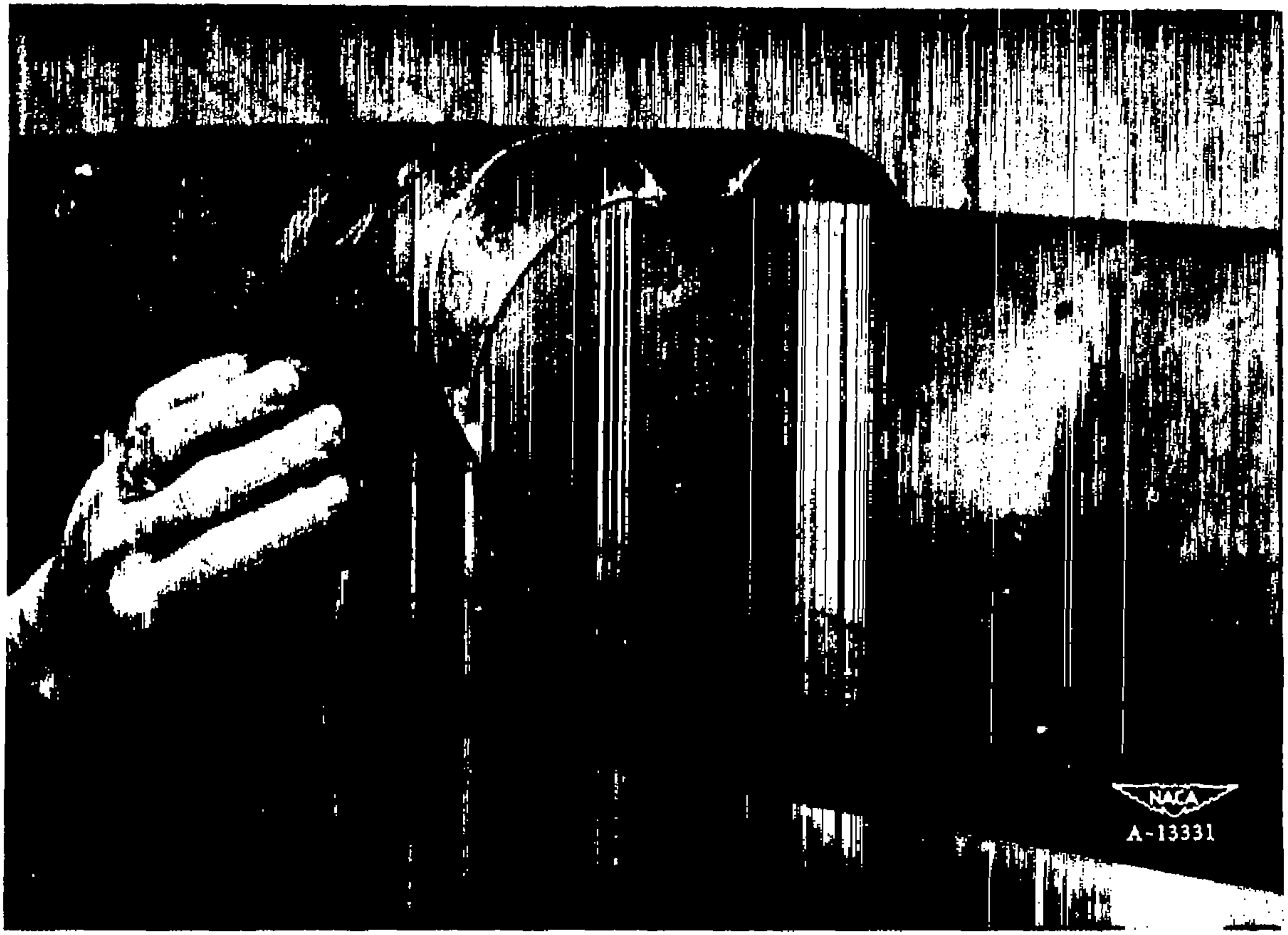

Figure 5.— Detail of the air scoops.

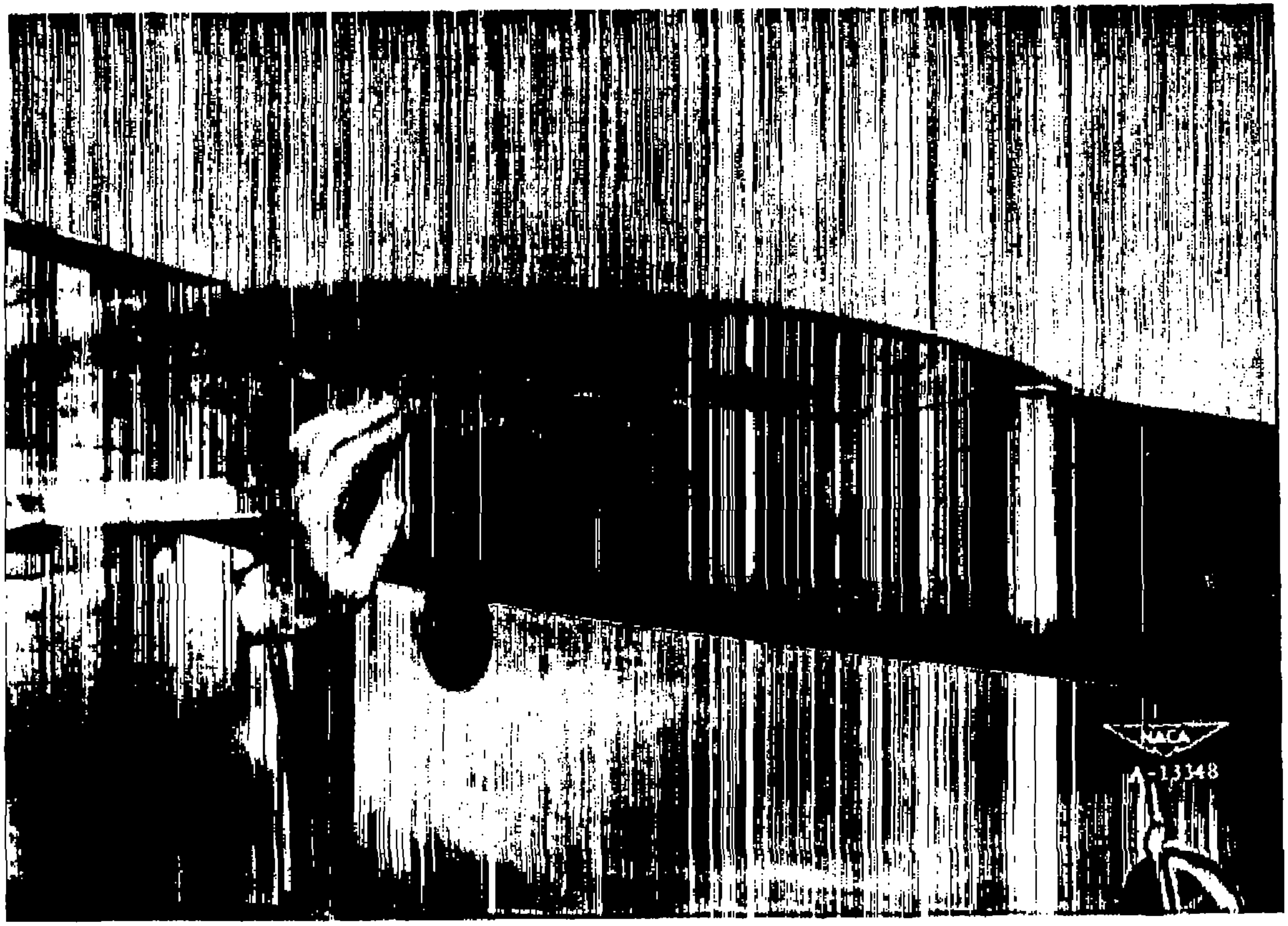

Figure 6.- Detail of the canopy.

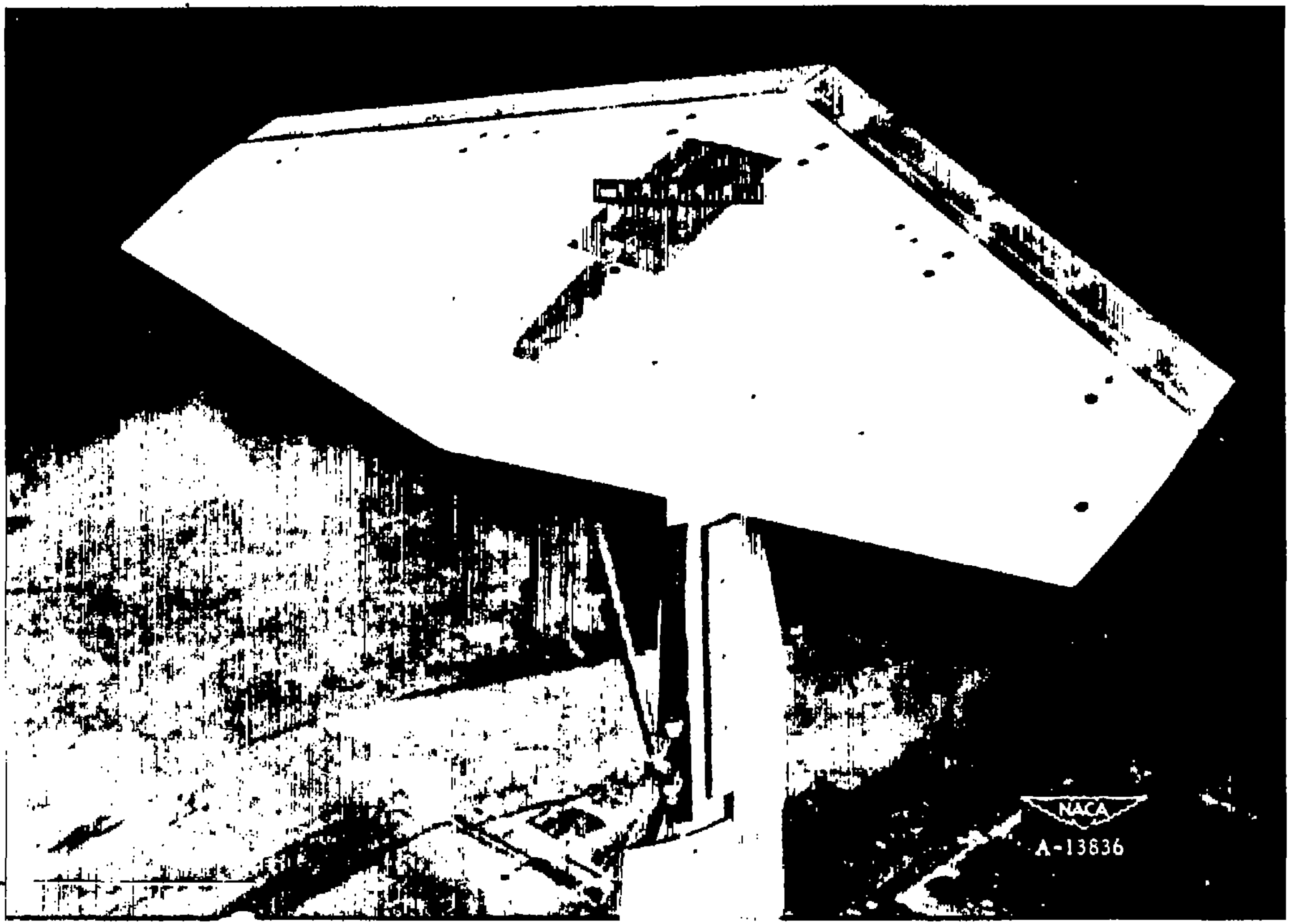

(a) Wing alone.

Figure 7.- The model mounted in the wind tunnel.

(b) Complete model with the flaps deflected, landing gear down, and main-gear-door configuration 2. $\delta_{LF} = 30^{\circ}$; $\delta_{TF} = 50^{\circ}$.

Figure 7.– Continued.

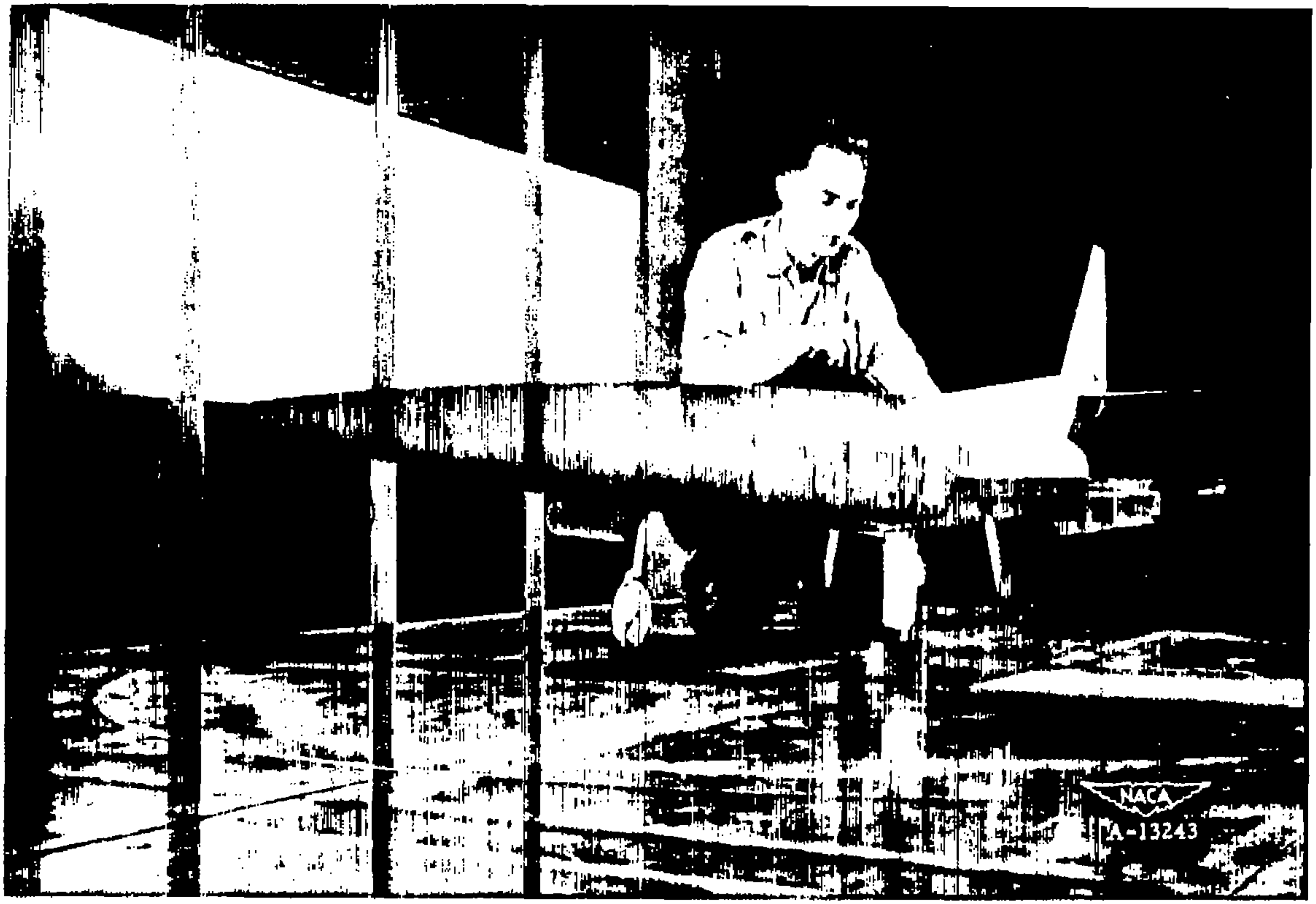

(c) Complete model with the flaps deflected and the landing gear down in the presence of the ground plane. $\delta_{LF} = 30^\circ$; $\delta_{TF} = 50^\circ$.

Figure 7.– Concluded.

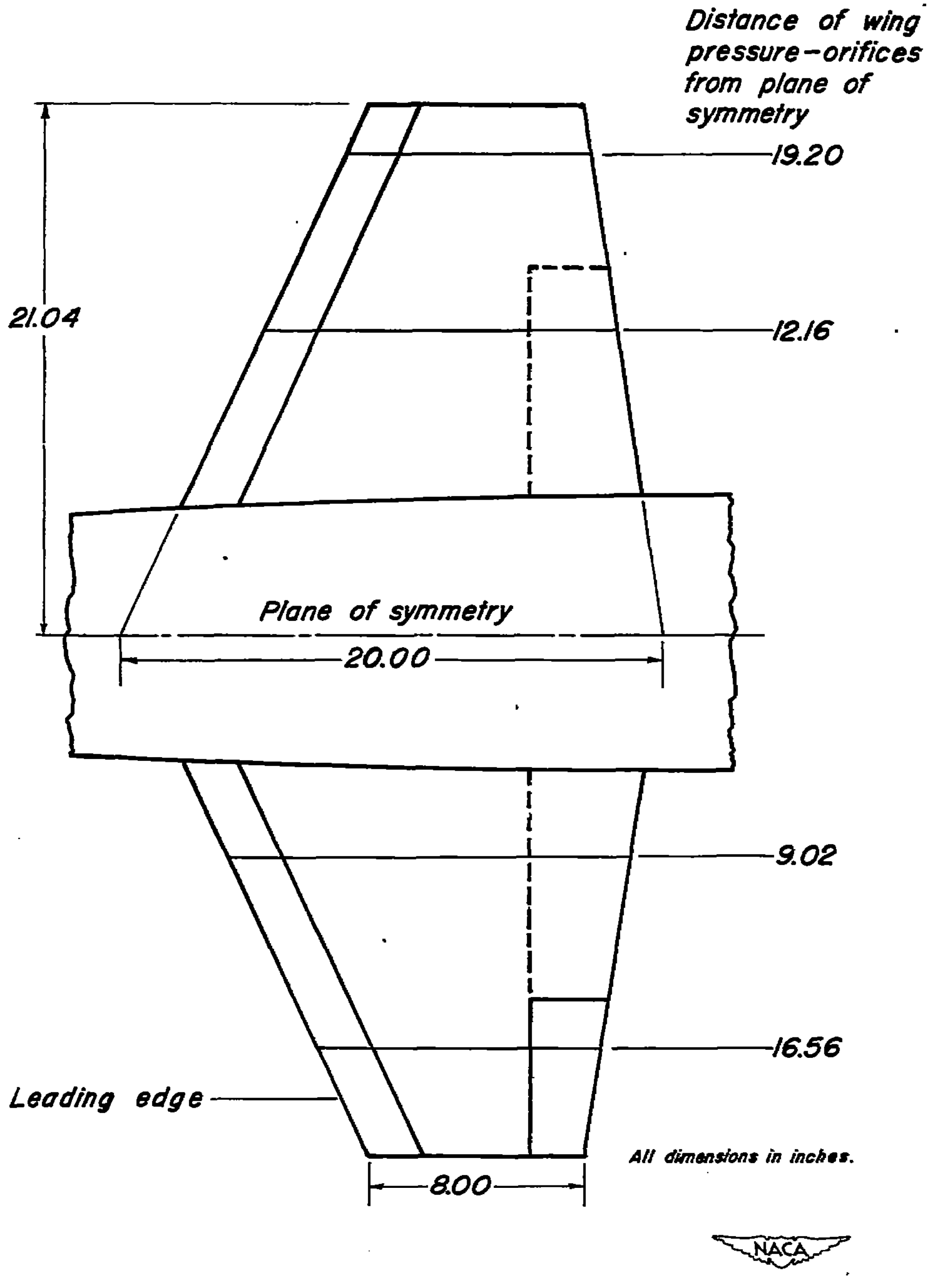

Figure 8.– Spanwise locations of the wing pressure orifices.

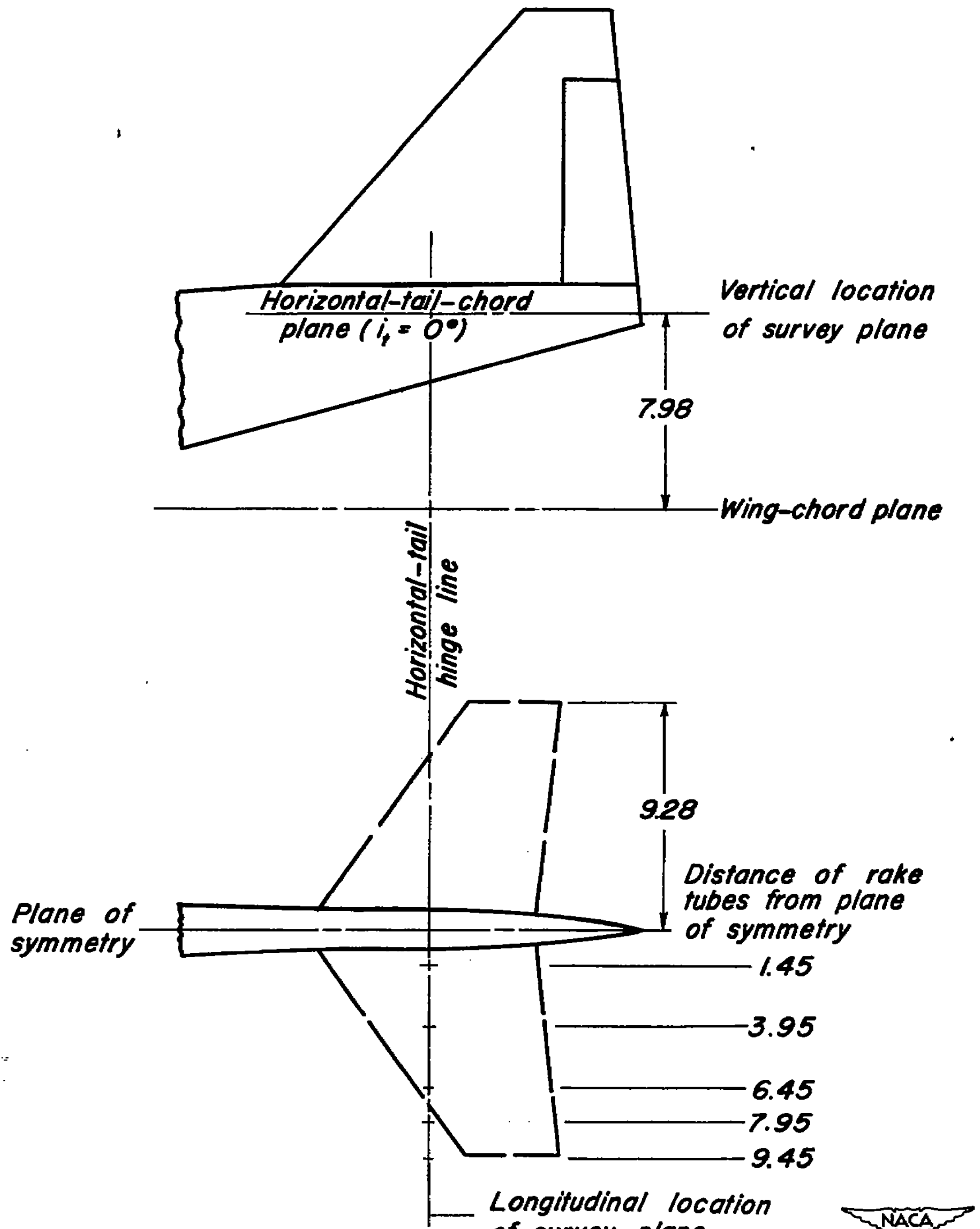

All dimensions in inches.

Figure 9.— Locations of the rake tubes used to measure the downwash and the dynamic pressure at the tail.

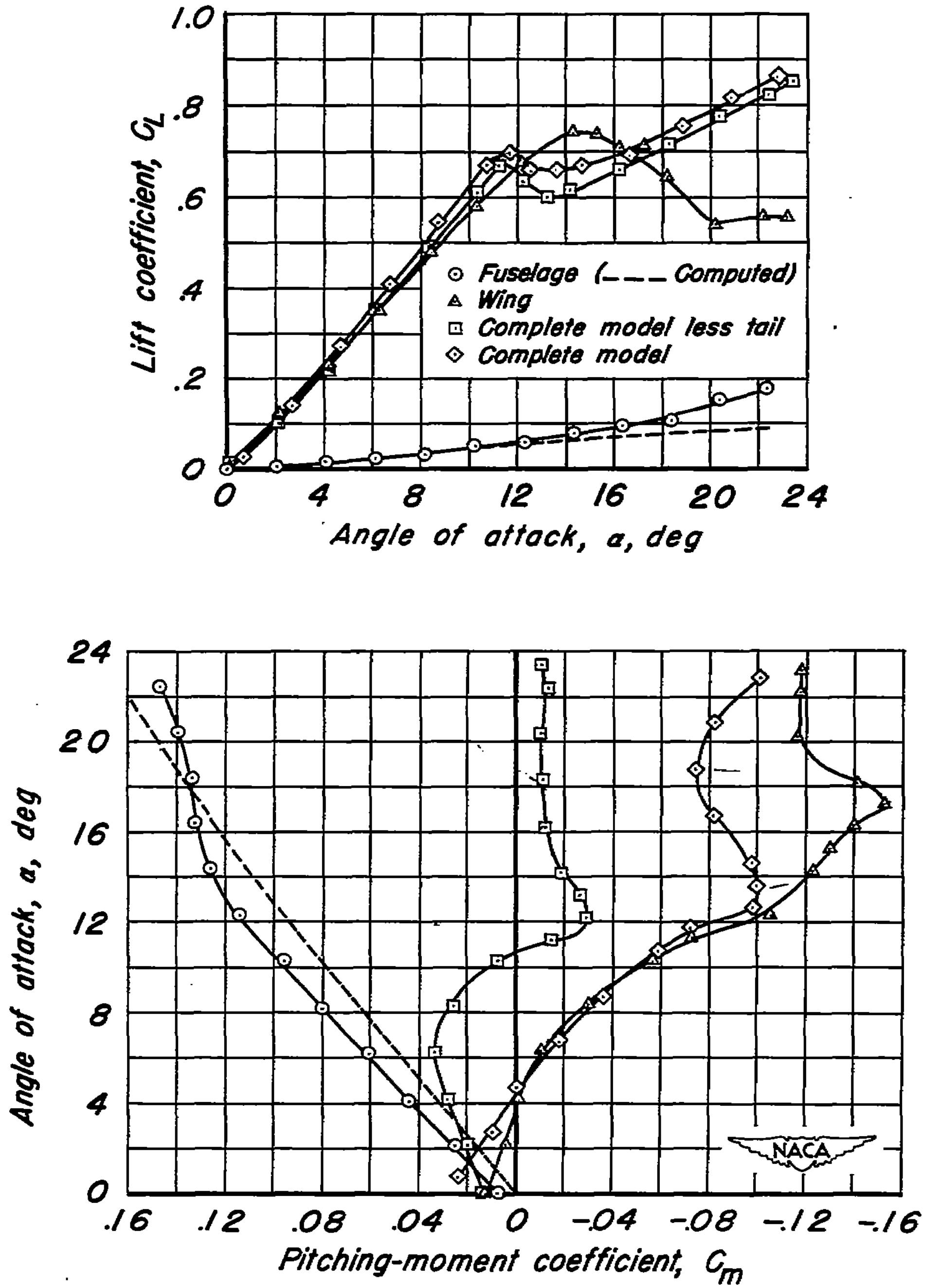

Figure 10.– Longitudinal characteristics of the complete model, of the complete model less tail, of the fuselage alone, and of the wing alone. Flaps neutral.

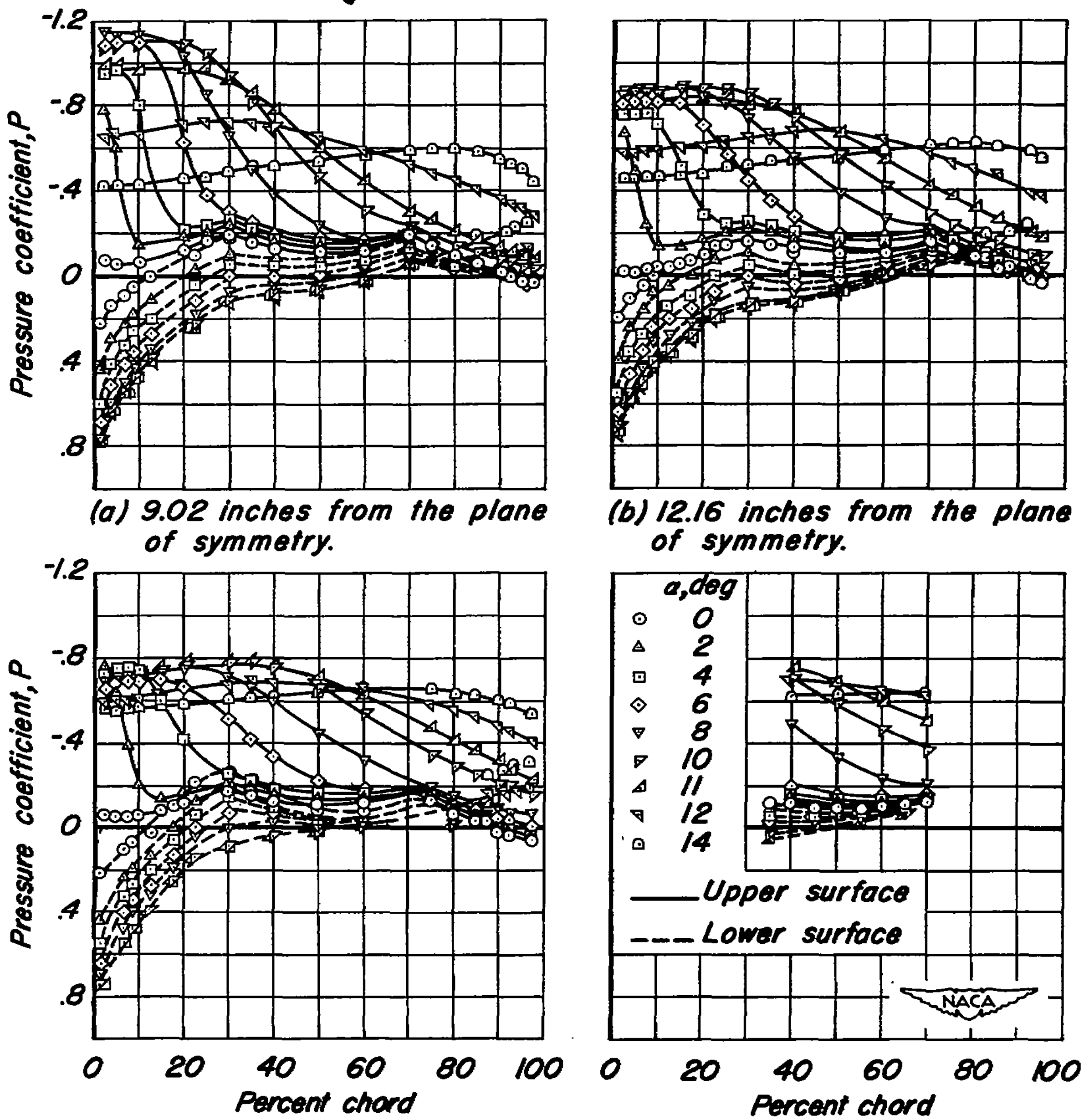

(a) 9.02 inches from the plane of symmetry.

(b) 12.16 inches from the plane of symmetry.

(c) 16.56 inches from the plane of symmetry.

(d) 19.20 inches from the plane of symmetry.

Figure 11.– Variation of the chordwise distribution of wing pressure with angle of attack. Flaps neutral.

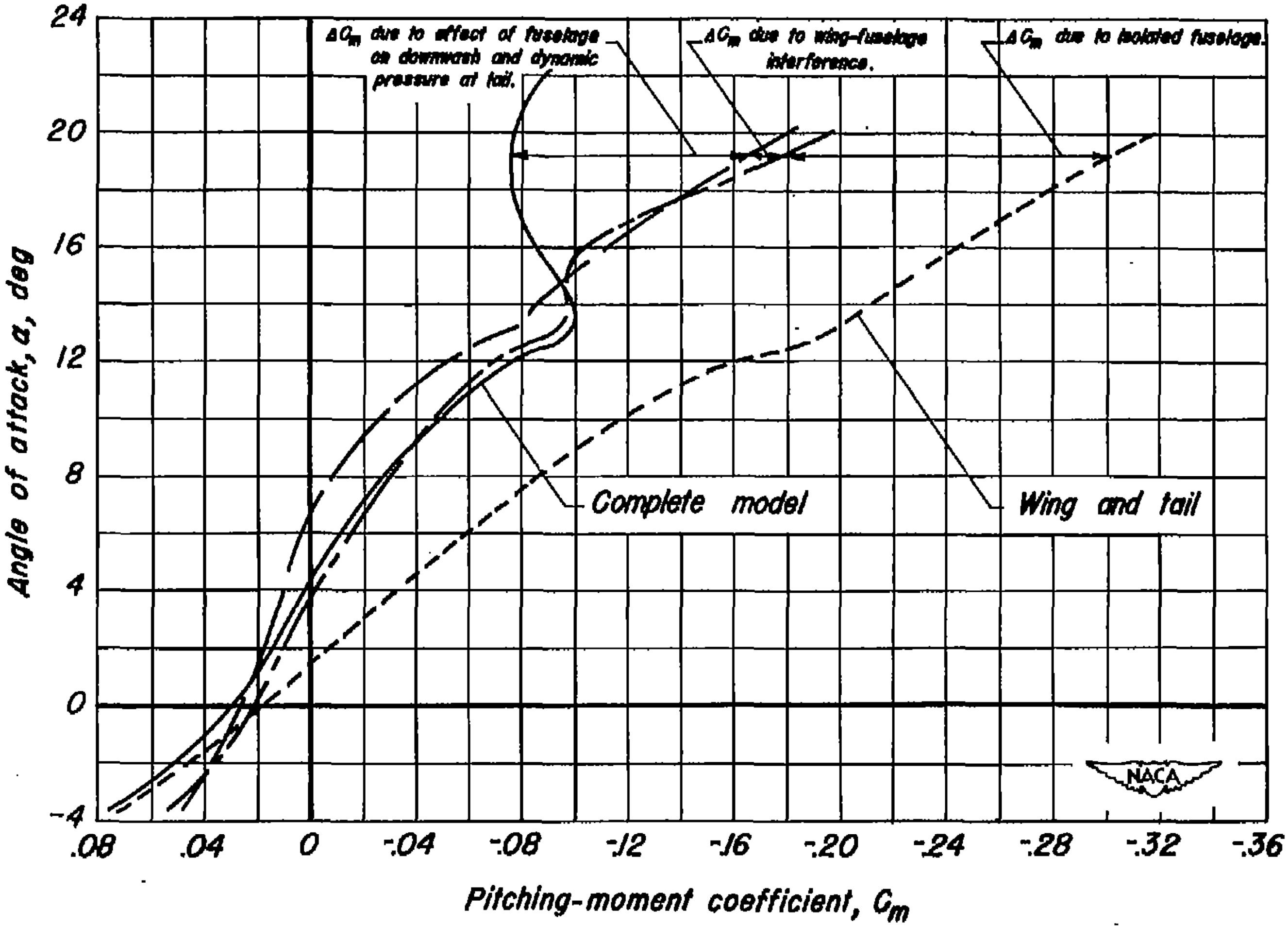

Figure 12.—The effects of the fuselage on the variation of the pitching-moment coefficient of the complete model with angle of attack. Flaps neutral.

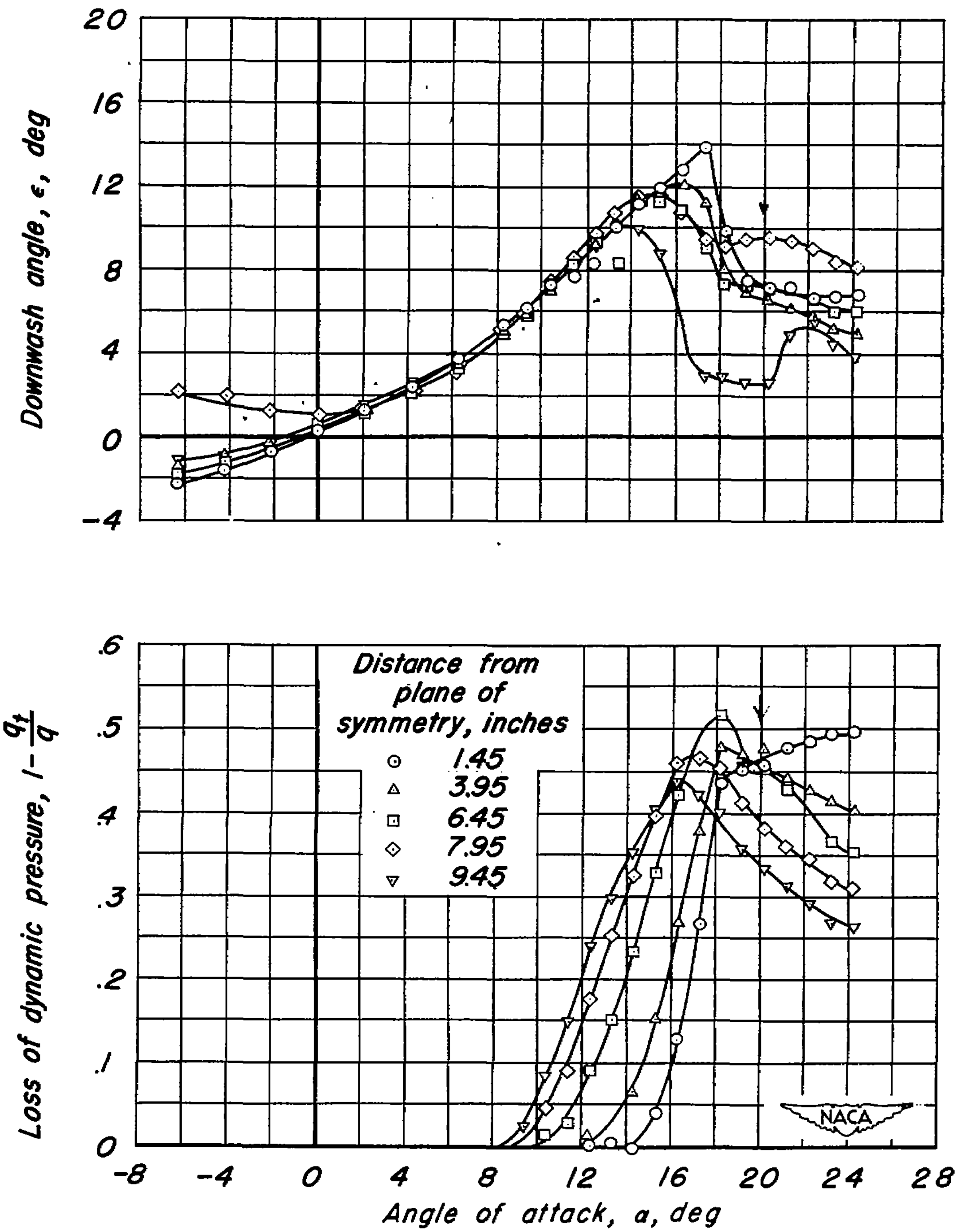

Figure 13.– Variation of the downwash and loss of dynamic pressure in the plane of the horizontal tail with angle of attack for the wing alone. Flaps neutral.

[redacted]

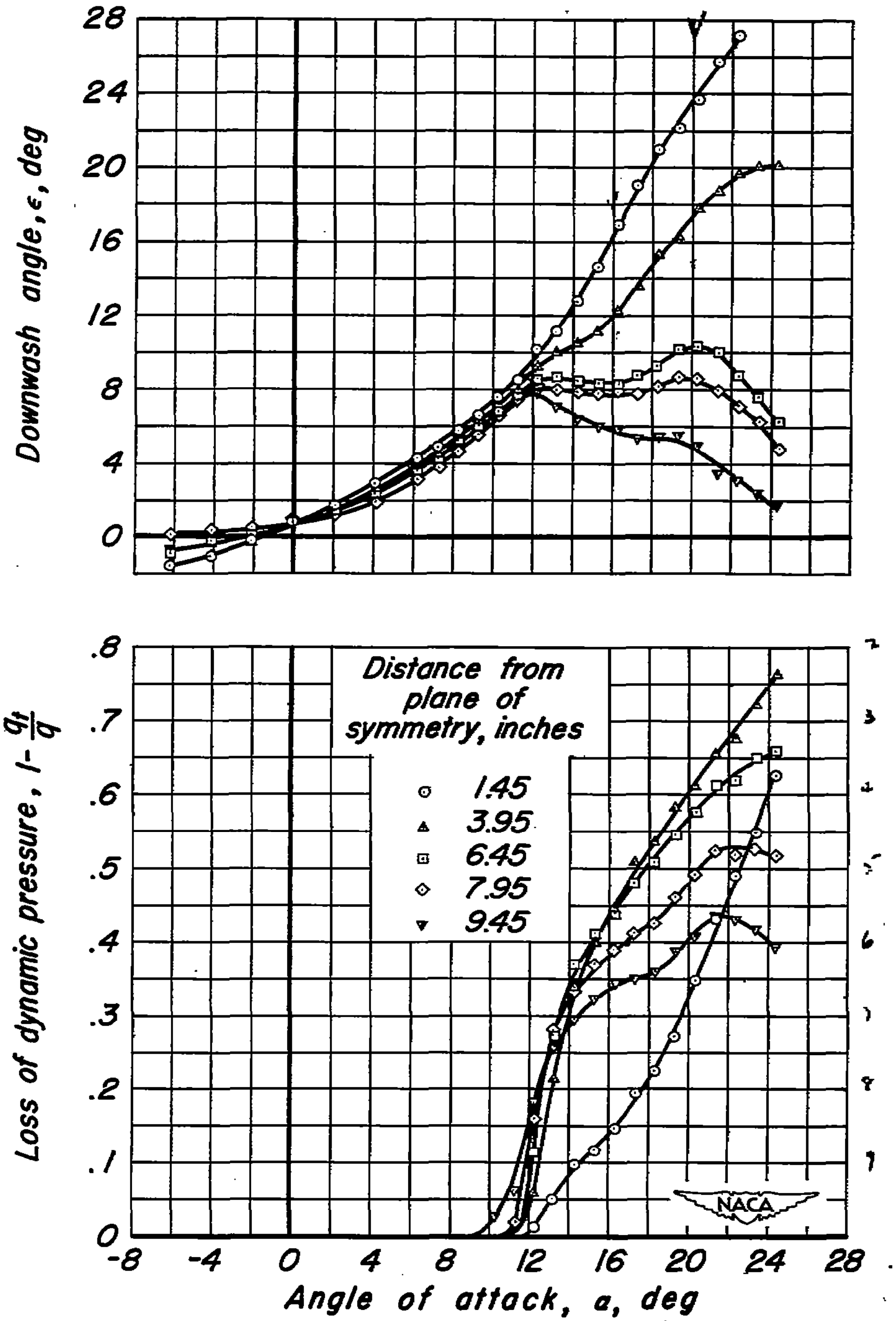

Figure 14.– Variation of the downwash and loss of dynamic pressure in the plane of the horizontal tail with angle of attack for the complete model less tail. Flaps neutral.

[redacted]

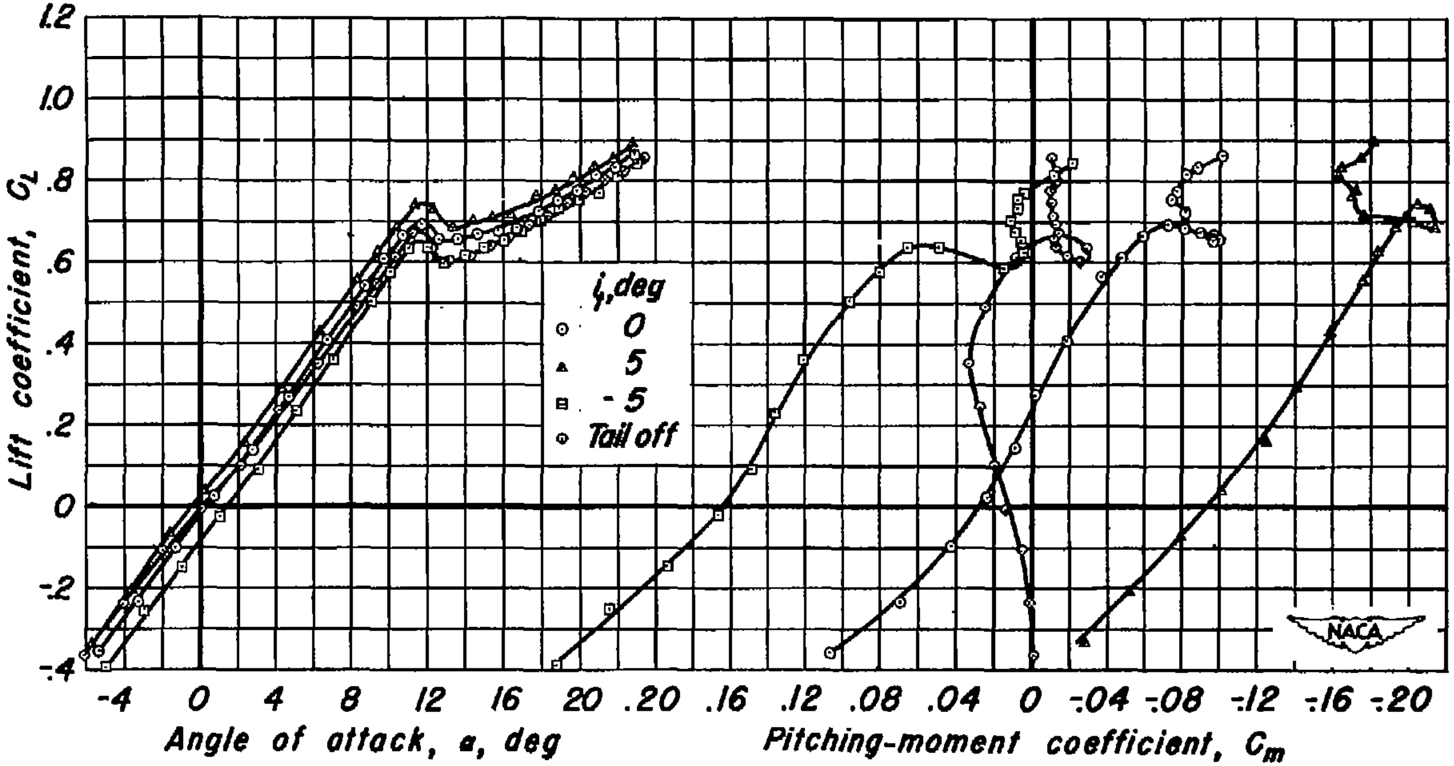

Figure 15.– The effect of the incidence of the horizontal tail on the longitudinal characteristics of the complete model. Flaps neutral.

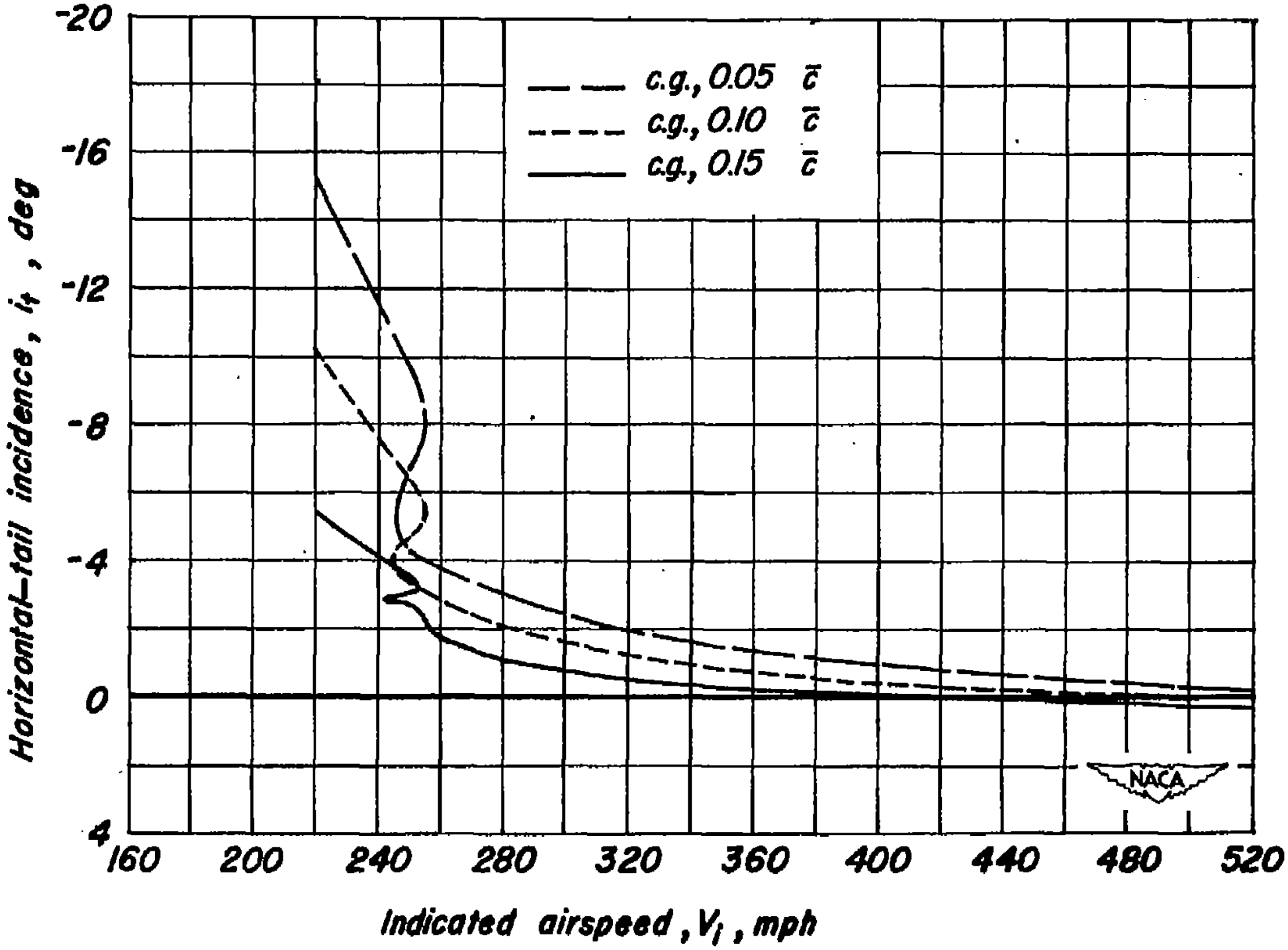

Figure 16.—Estimated variation of the incidence of the horizontal tail with indicated airspeed for the airplane in steady, straight, unyawed flight. Flaps neutral.

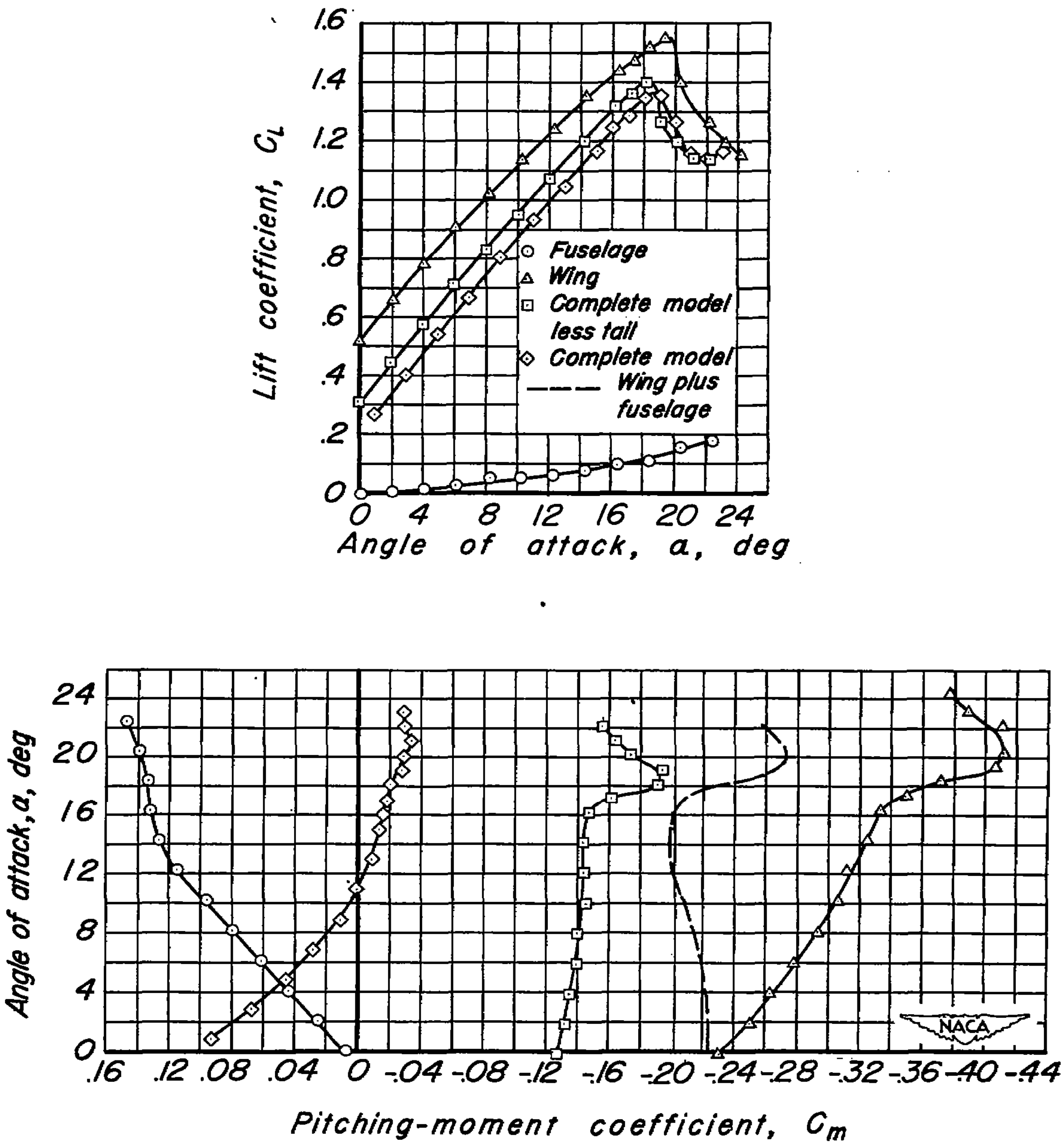

Figure 17.– Longitudinal characteristics of the complete model, of the complete model less tail, of the fuselage alone, and of the wing alone. $\delta_{LF} = 30°$, $\delta_{TF} = 50°$.

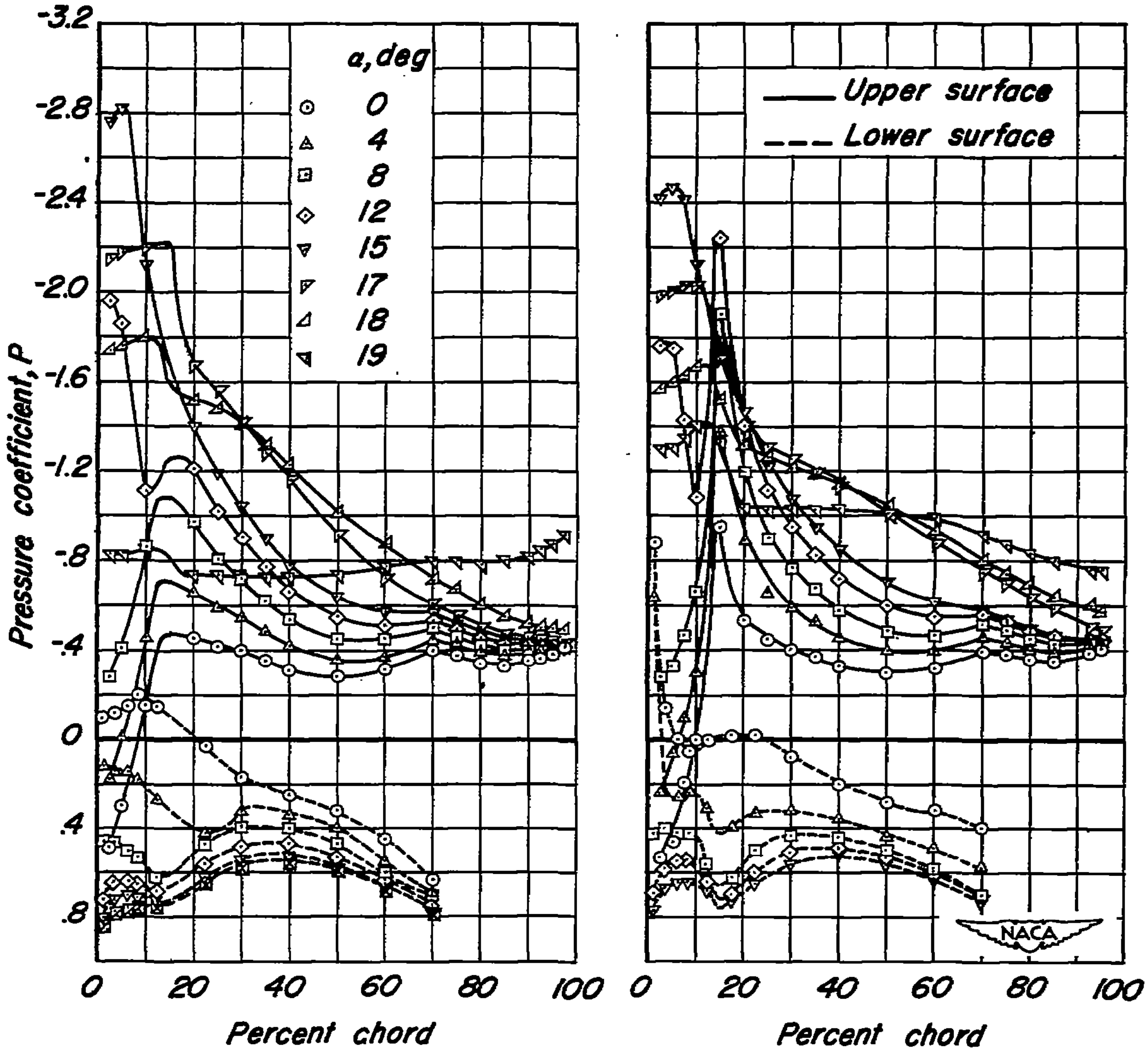

(a) 9.02 inches from the plane of symmetry.

(b) 12.16 inches from the plane of symmetry.

Figure 18.– Variation of the chordwise distribution of wing pressure with angle of attack. $\delta_{LF} = 30°$, $\delta_{TF} = 50°$.

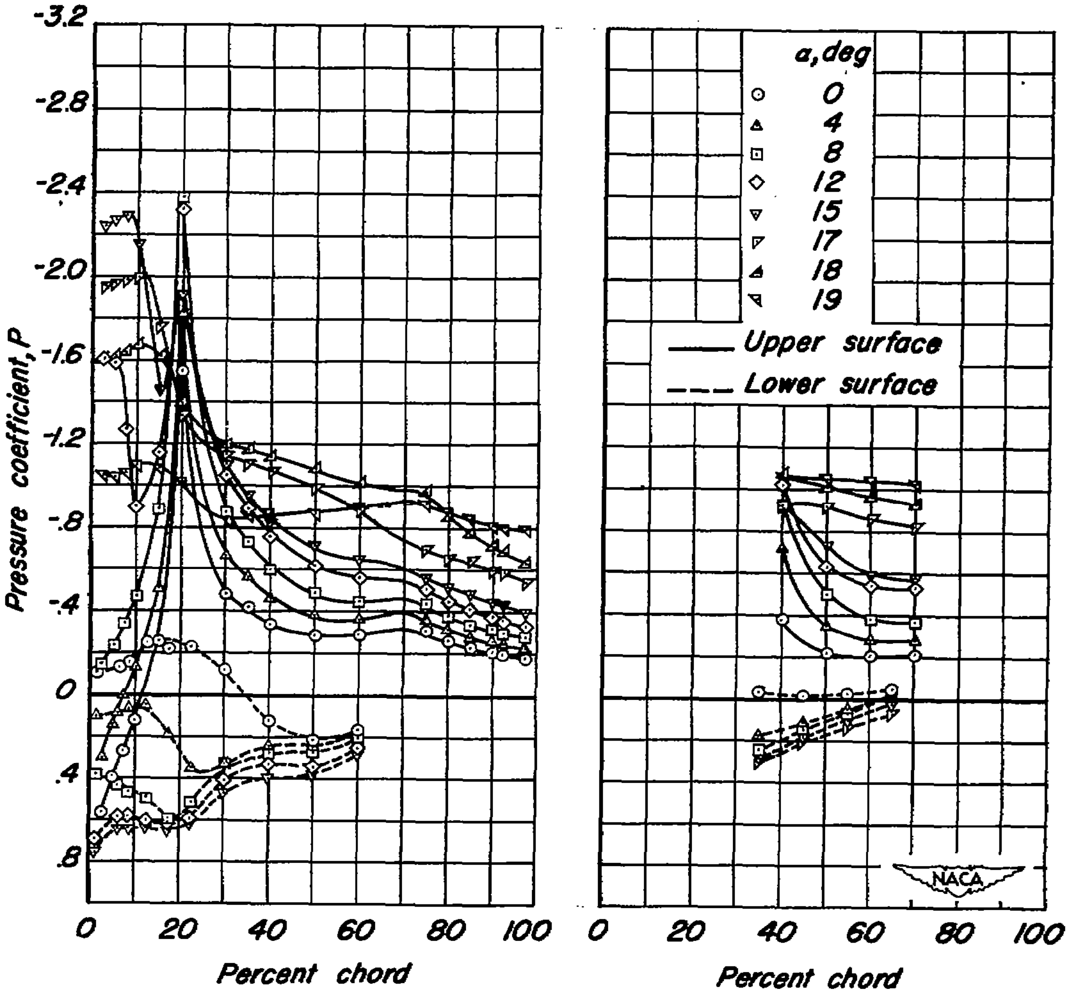

(c) 16.56 inches from the plane of symmetry.

(d) 19.20 inches from the plane of symmetry.

Figure 18.— Concluded.

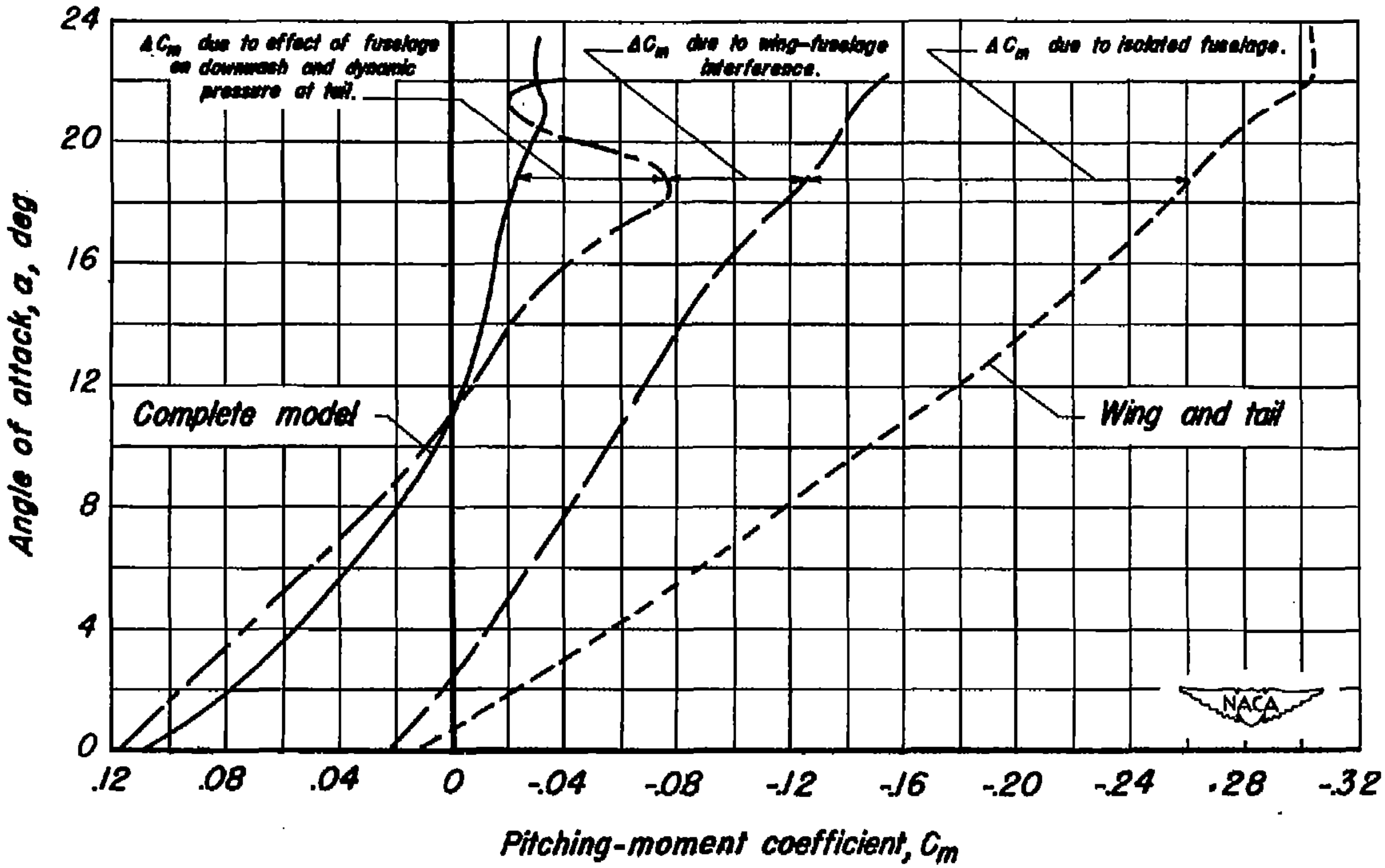

Figure 19.– The effects of the fuselage on the variation of the pitching-moment coefficient of the complete model with angle of attack. $\delta_{LF}=30°$, $\delta_{TF}=50°$.

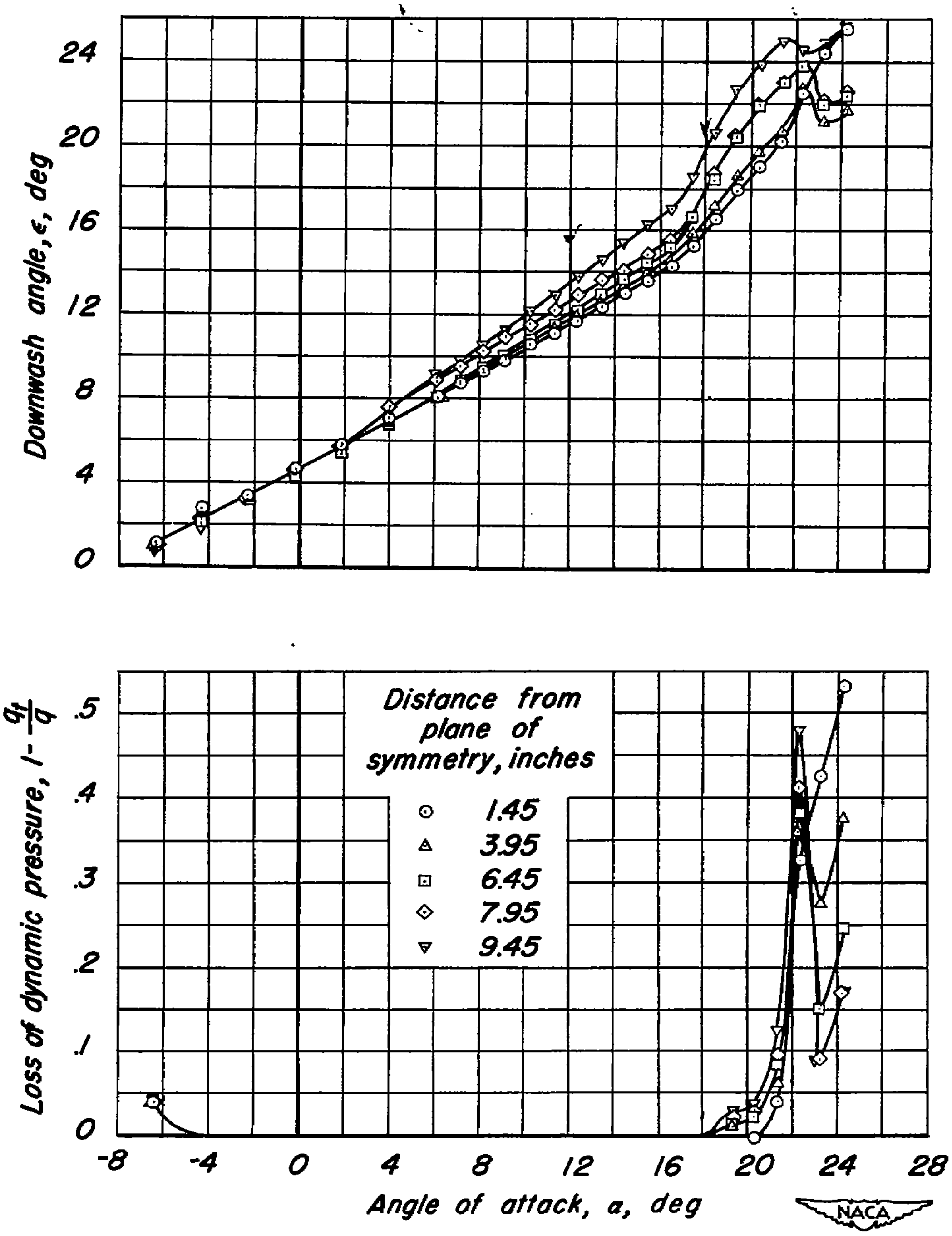

Figure 20.– Variation of the downwash and loss of dynamic pressure in the plane of the horizontal tail with angle of attack for the wing alone. $\delta_{LF} = 30°$, $\delta_{TF} = 50°$.

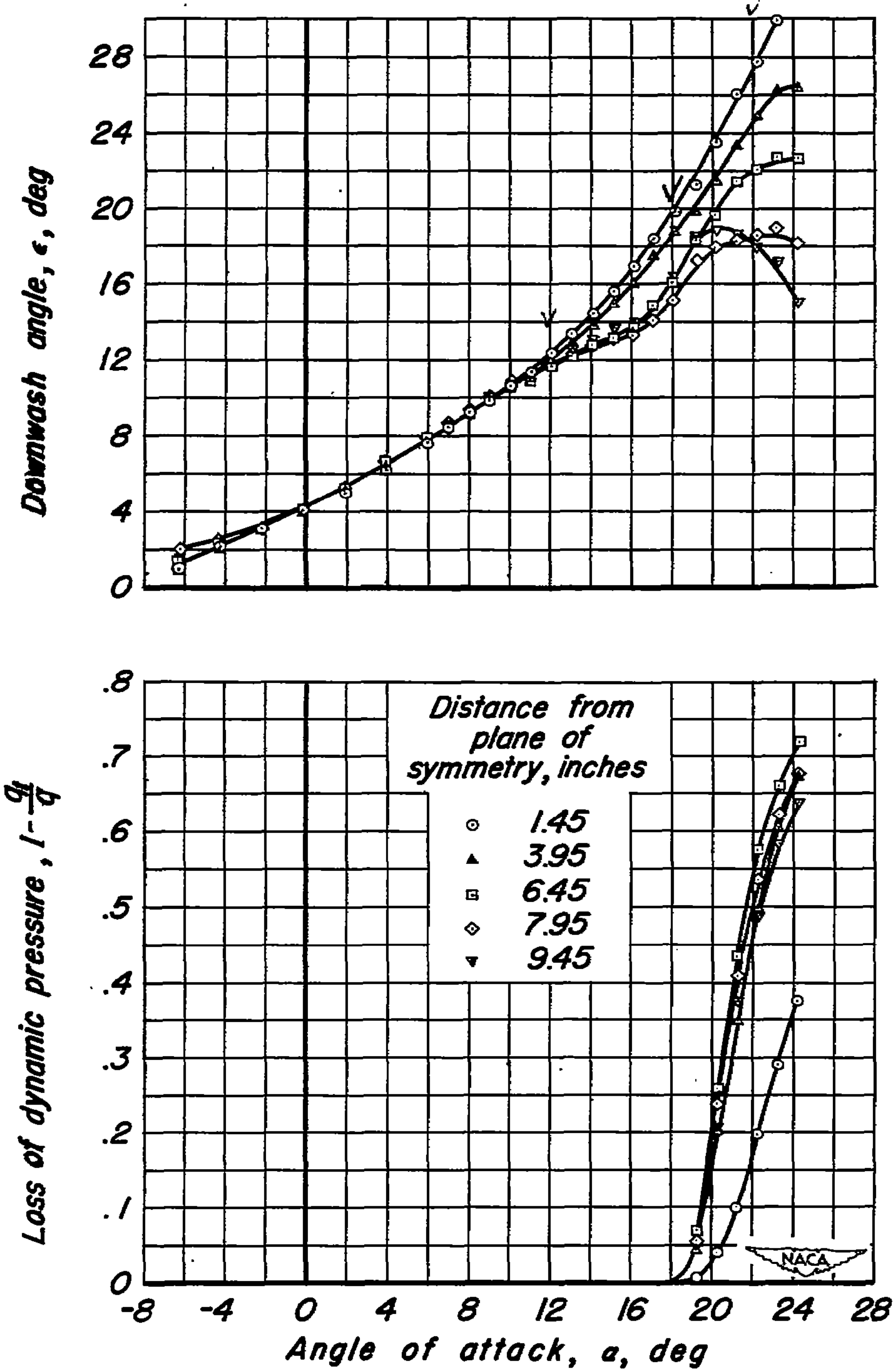

Figure 21.– Variation of the downwash and loss of dynamic pressure in the plane of the horizontal tail with angle of attack for the complete model less tail. $\delta_{LF} = 30°$, $\delta_{TF} = 50°$.

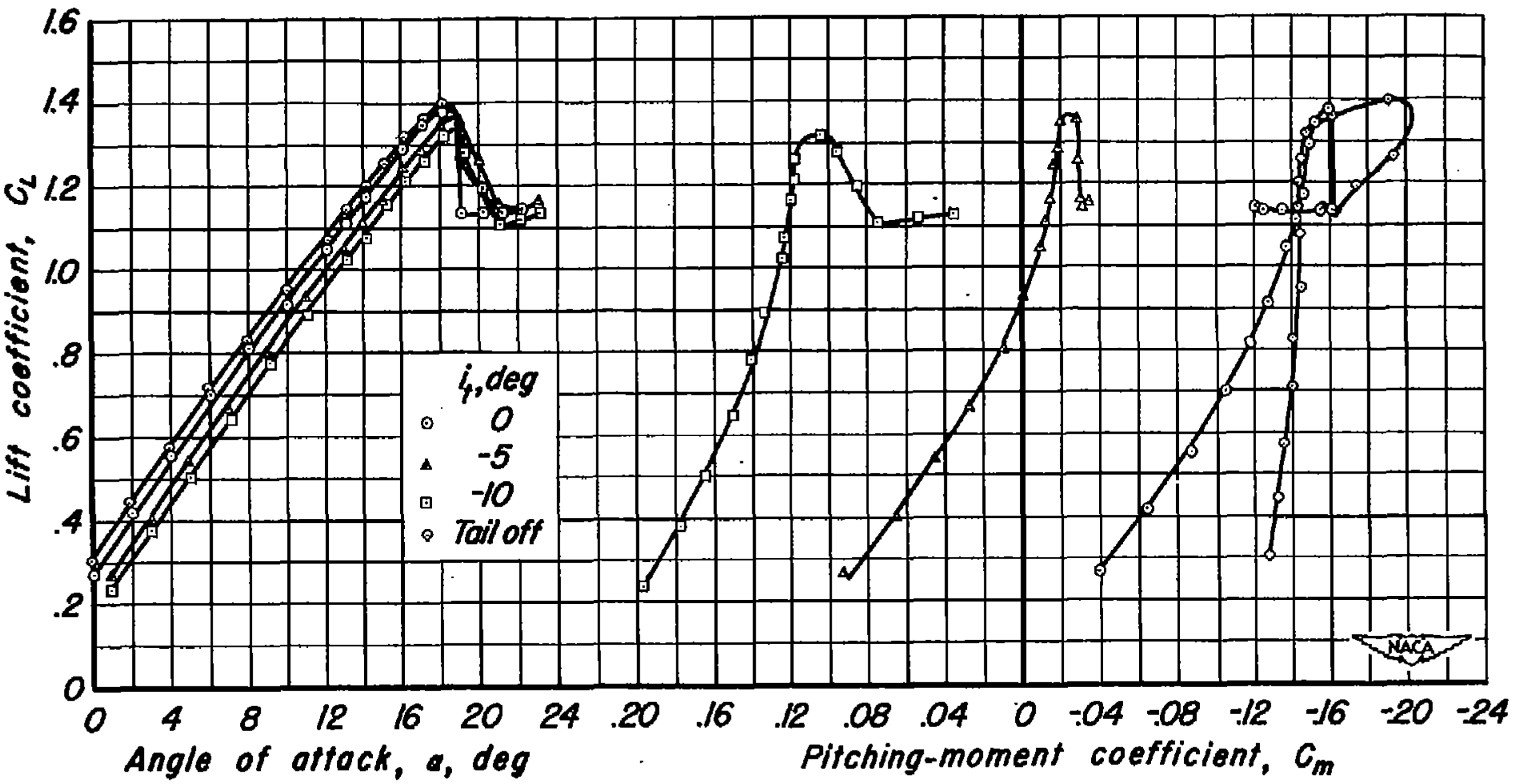

Figure 22.–The effect of the incidence of the horizontal tail on the longitudinal characteristics of the complete model. $\delta_{LF} = 30°$, $\delta_{TF} = 50°$

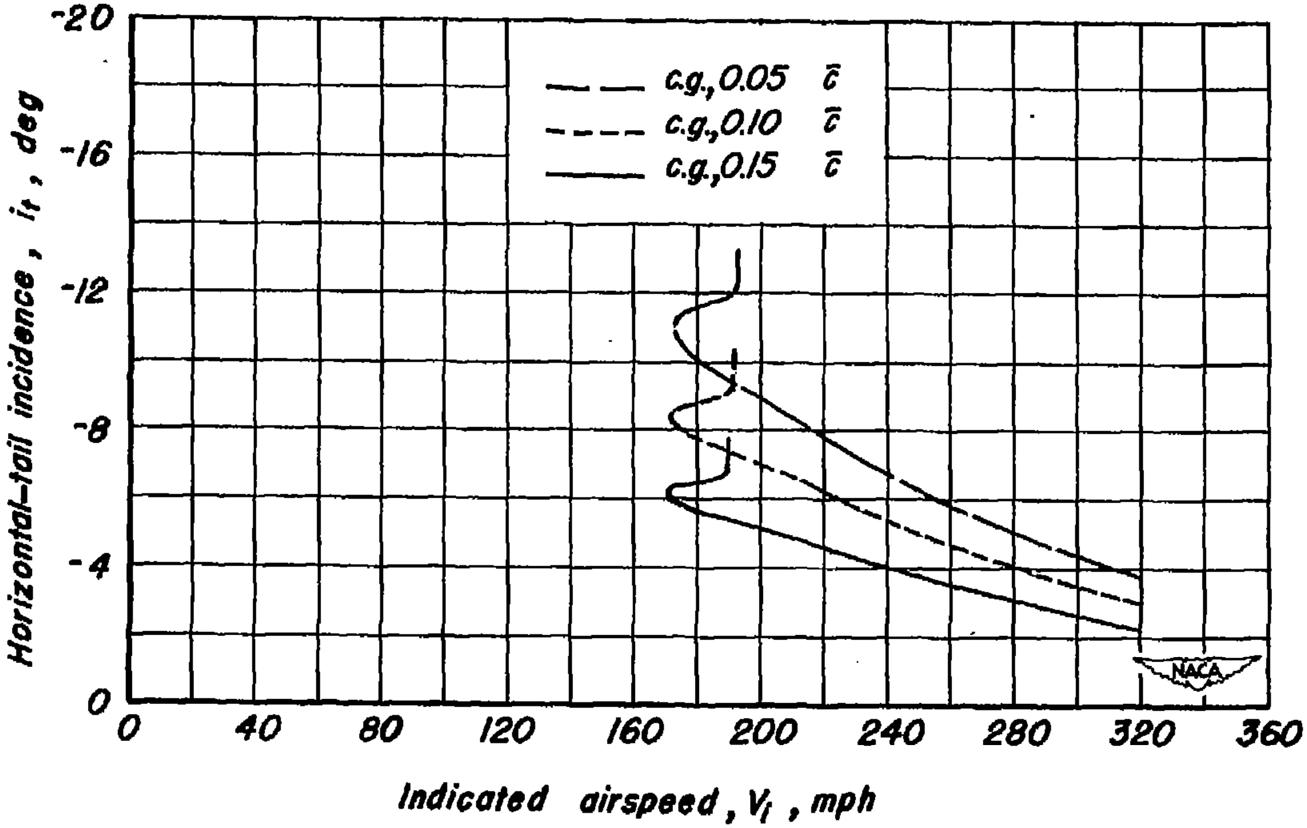

Figure 23.– Estimated variation of the incidence of the horizontal tail with indicated airspeed for the airplane in steady, straight, unyawed flight. $\delta_{LF}=30°$, $\delta_{TF}=50°$.

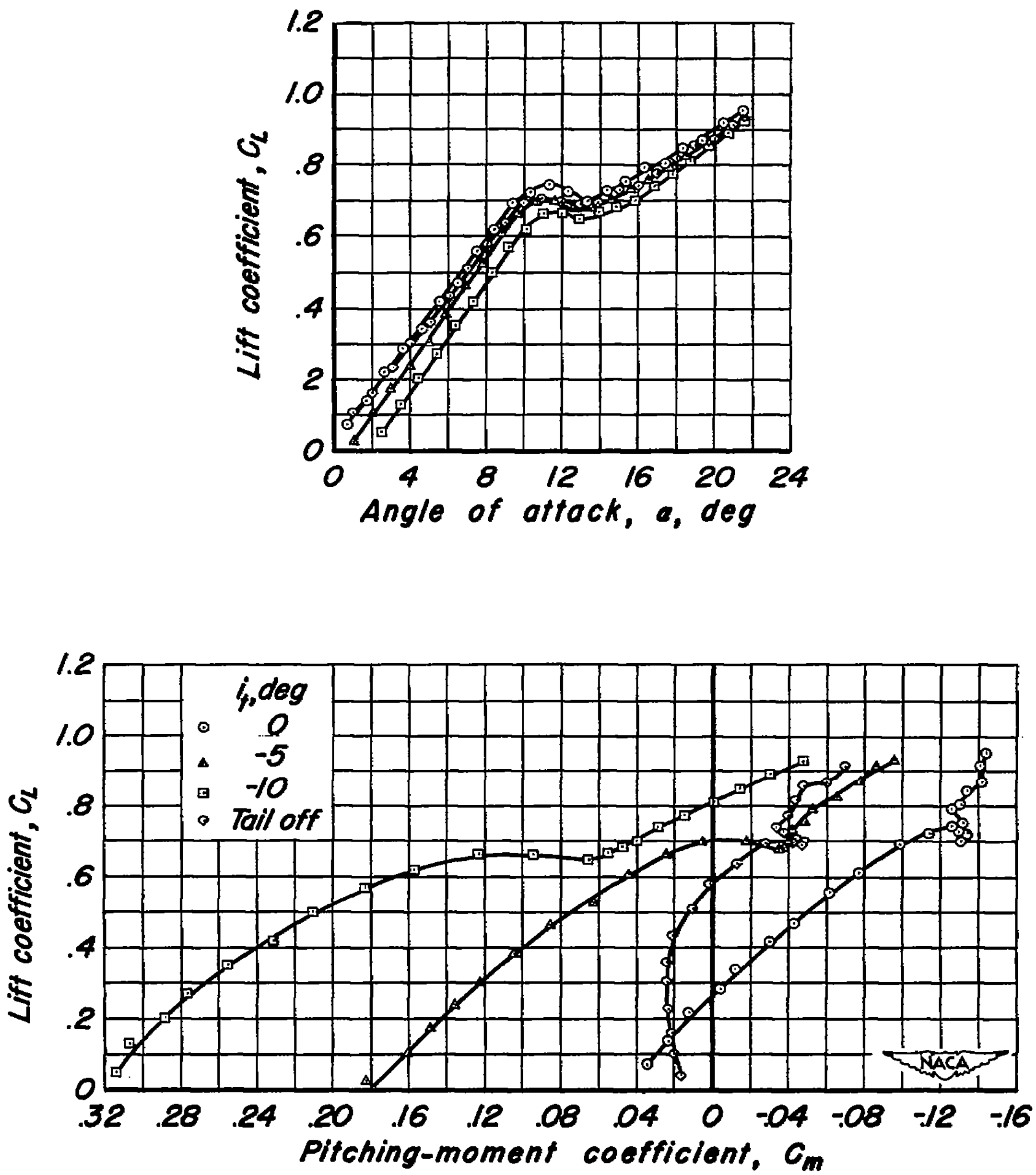

Figure 24.–The effect of the incidence of the horizontal tail on the longitudinal characteristics of the complete model in the presence of a ground plane. Flaps neutral; gear down, main gear doors off.

[redacted]

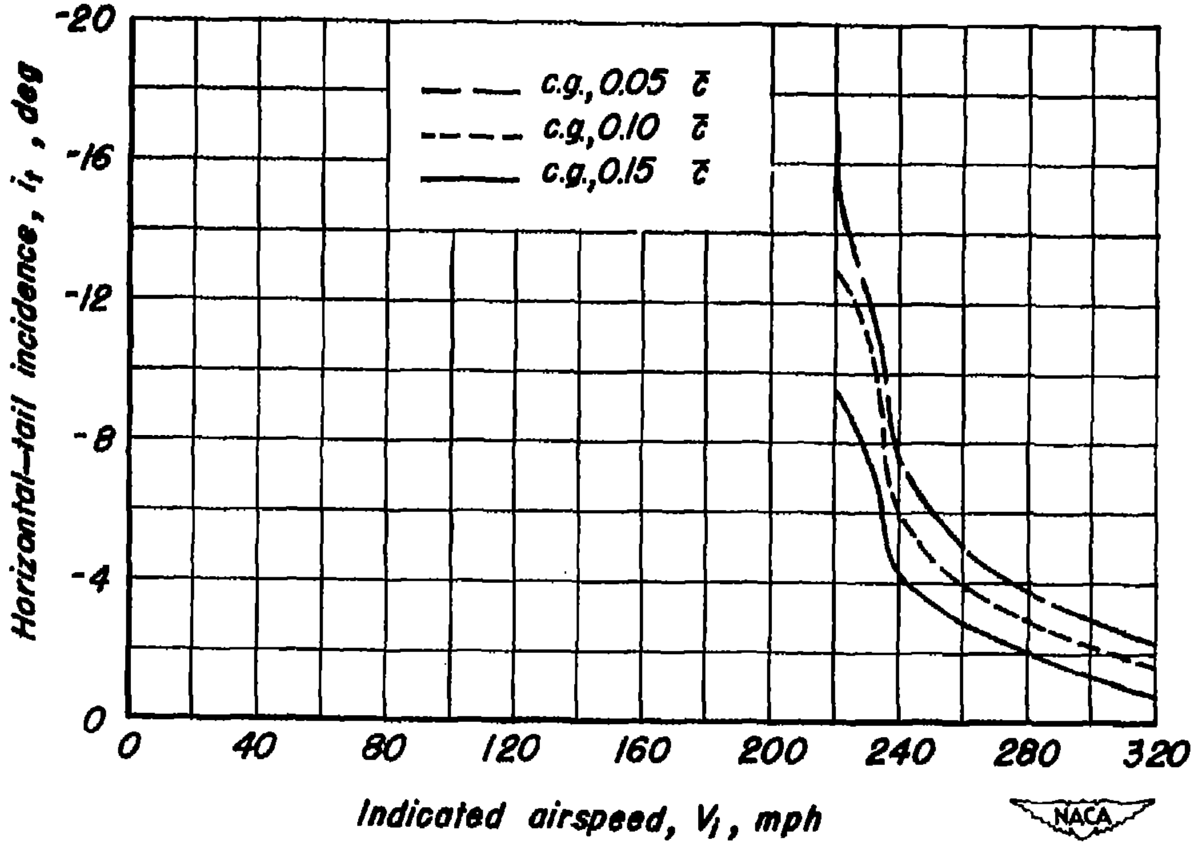

Figure 25.—Estimated variation of the incidence of the horizontal tail with indicated airspeed for the airplane in steady, straight, unyawed flight 0.28 wing span above the ground. Flaps neutral; gear down, main-gear doors off.

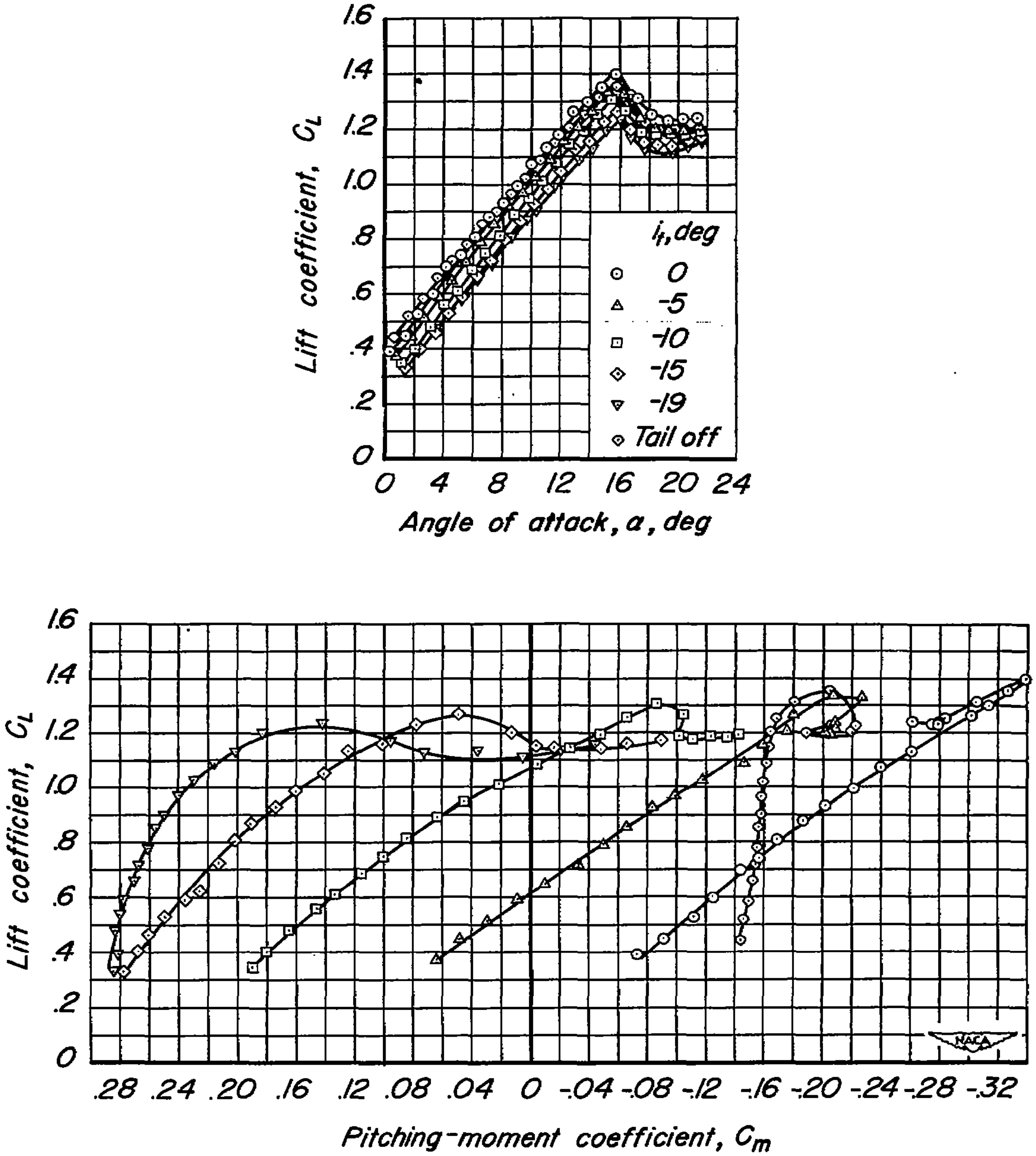

Figure 26.—The effect of the incidence of the horizontal tail on the longitudinal characteristics of the complete model in the presence of a ground plane. $\delta_{LF}=30°$, $\delta_{TF}=50°$; gear down, main-gear doors off.

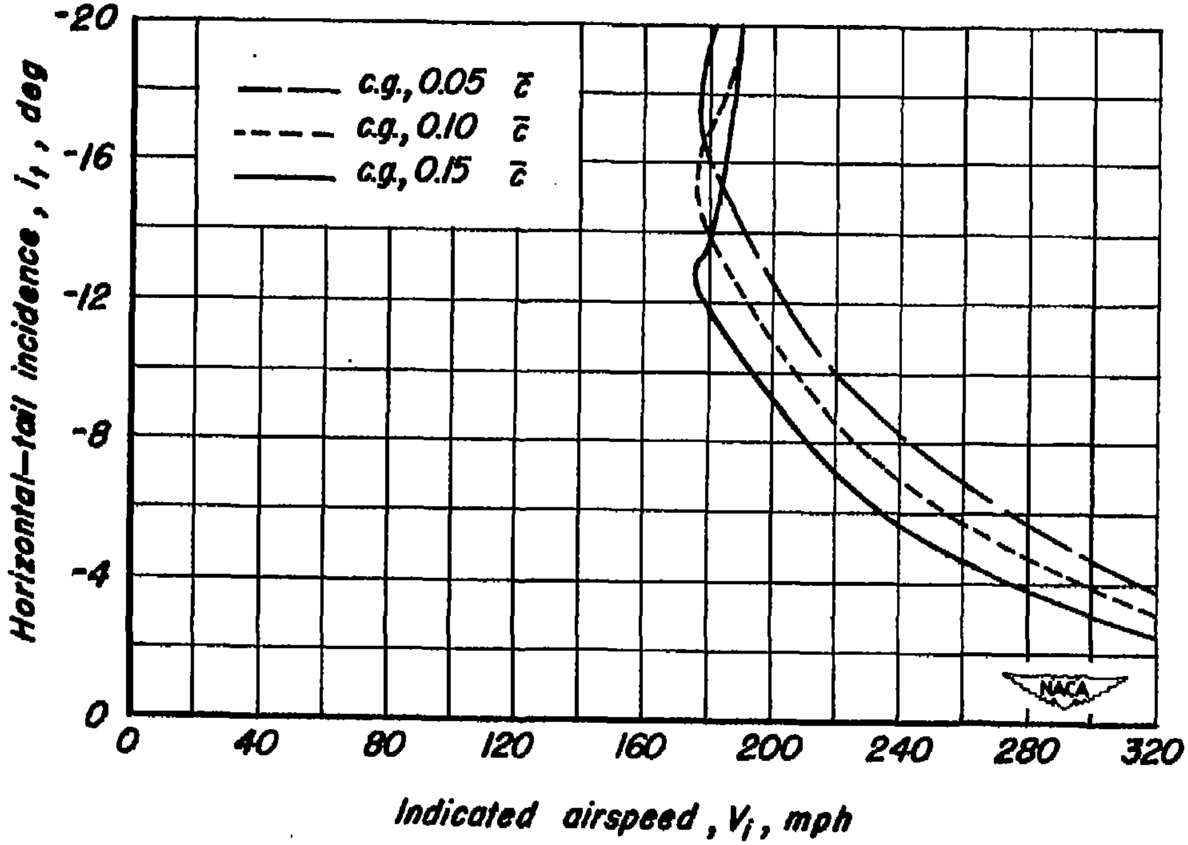

Figure 27.–Estimated variation of the incidence of the horizontal tail with indicated airspeed for the airplane in steady, straight, unyawed flight 0.28 wing span above the ground. δ_{LF}=30°, δ_{TF}=50°; gear down, main-gear doors off.

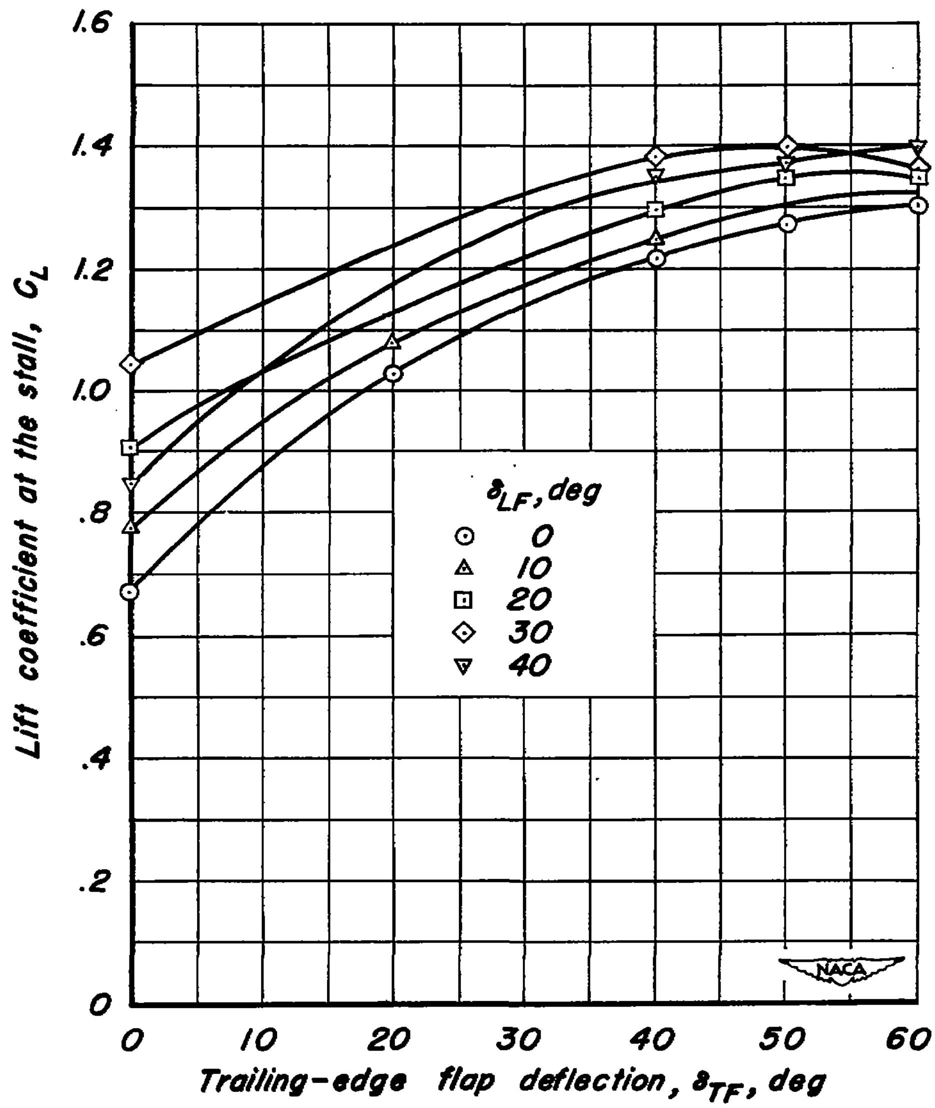

Figure 28.— Variation of the lift coefficient at the stall with leading- and trailing-edge flap deflections for the complete model less tail.

[redacted]

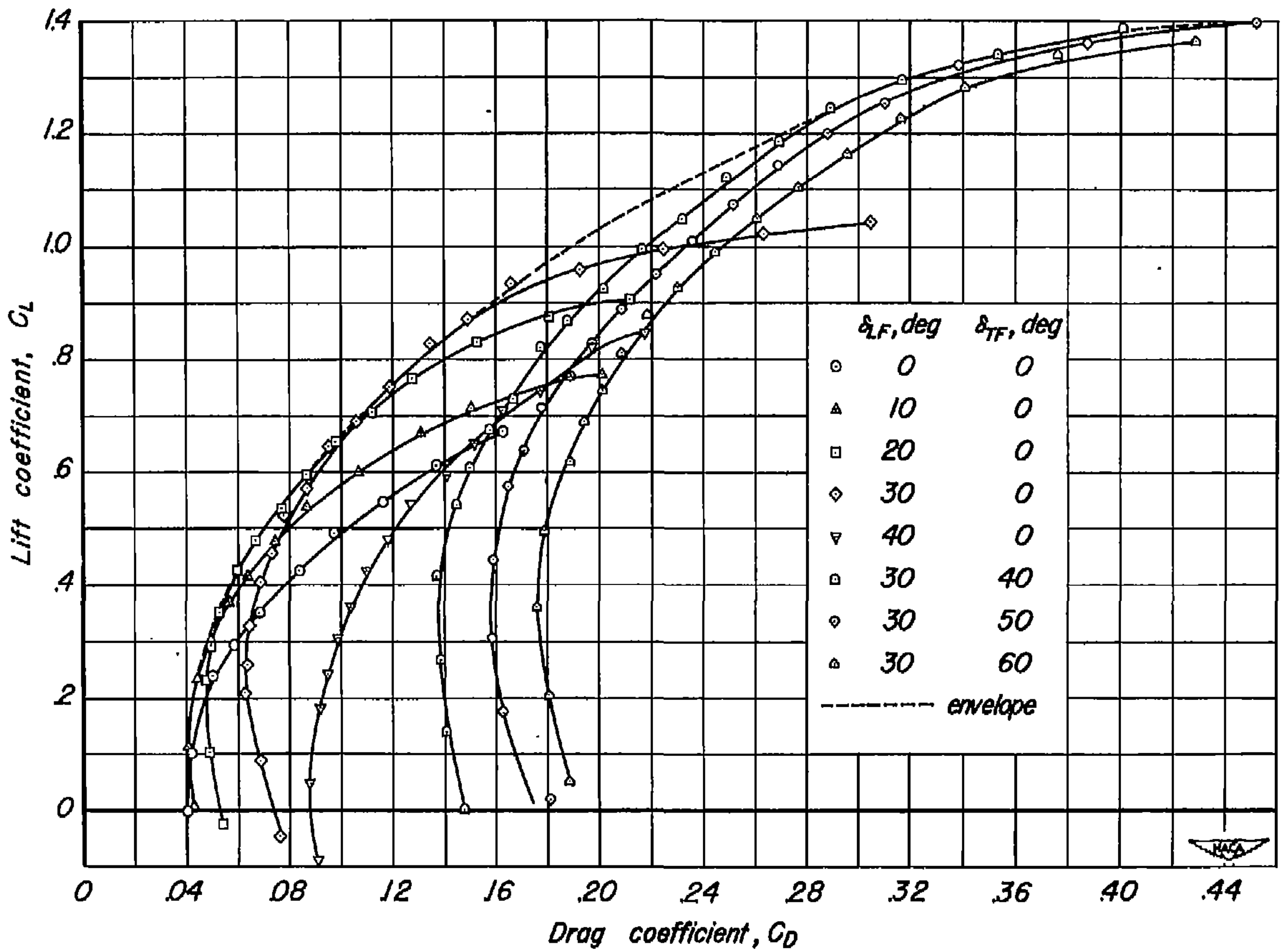

Figure 29.– The effect of leading- and trailing-edge flap deflections on the variation of the drag coefficient with lift coefficient for the complete model less tail.

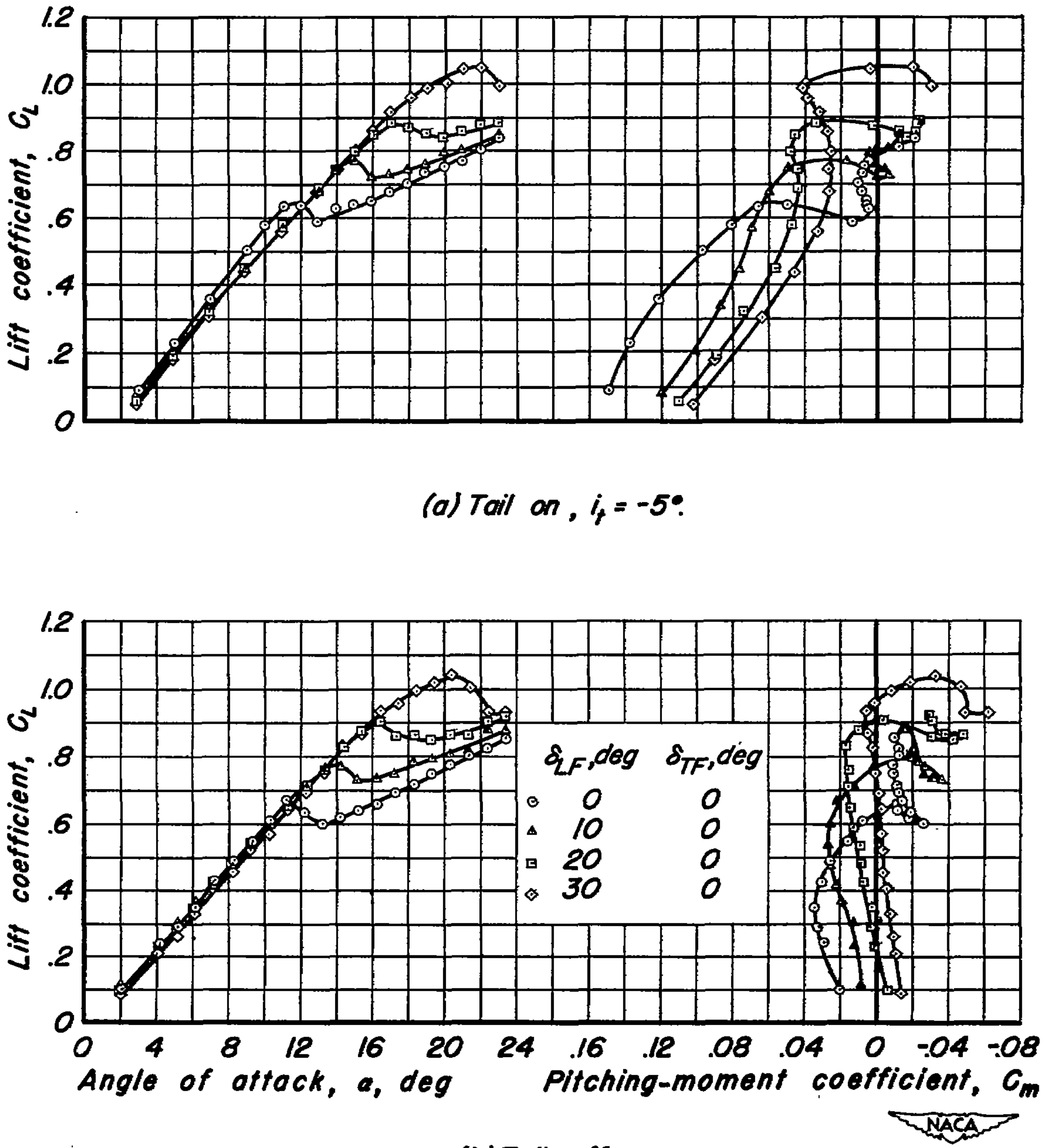

(a) Tail on, $i_t = -5°$.

(b) Tail off.

Figure 30.—The effect of leading-edge flap deflection on the longitudinal characteristics of the complete model.

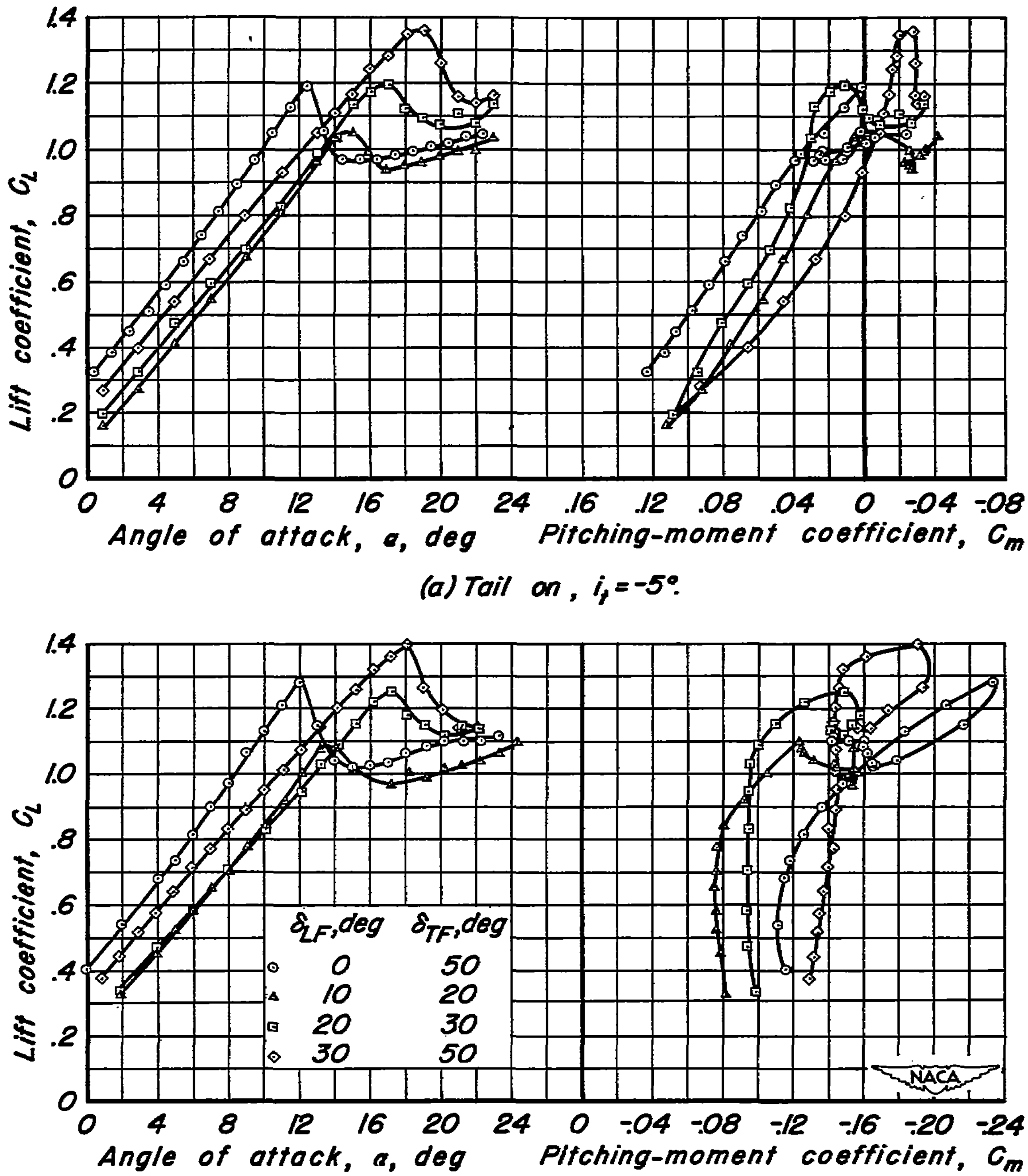

(a) Tail on, $i_t = -5°$.

(b) Tail off.

Figure 31.–The effect of leading- and trailing-edge flap deflections on the longitudinal characteristics of the complete model.

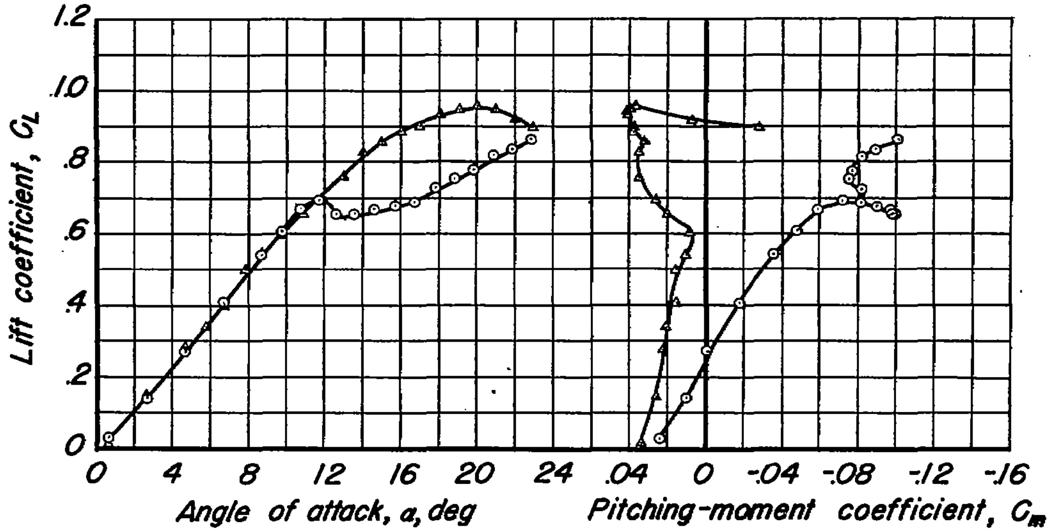

(a) Flaps neutral ; $i_t = 0°$.

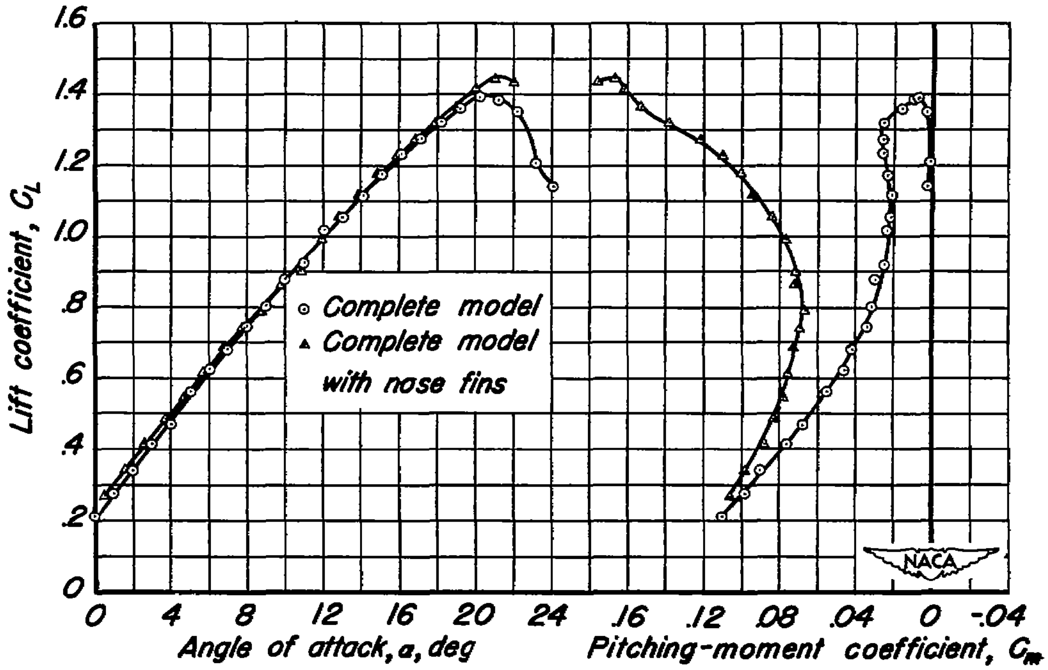

(b) $\delta_{LF} = 30°$, $\delta_{TF} = 50°$; $i_t = -5°$; gear down with main-gear-door configuration I.

Figure 32.–The effect of the nose fins on the longitudinal characteristics of the complete model.

[redacted]

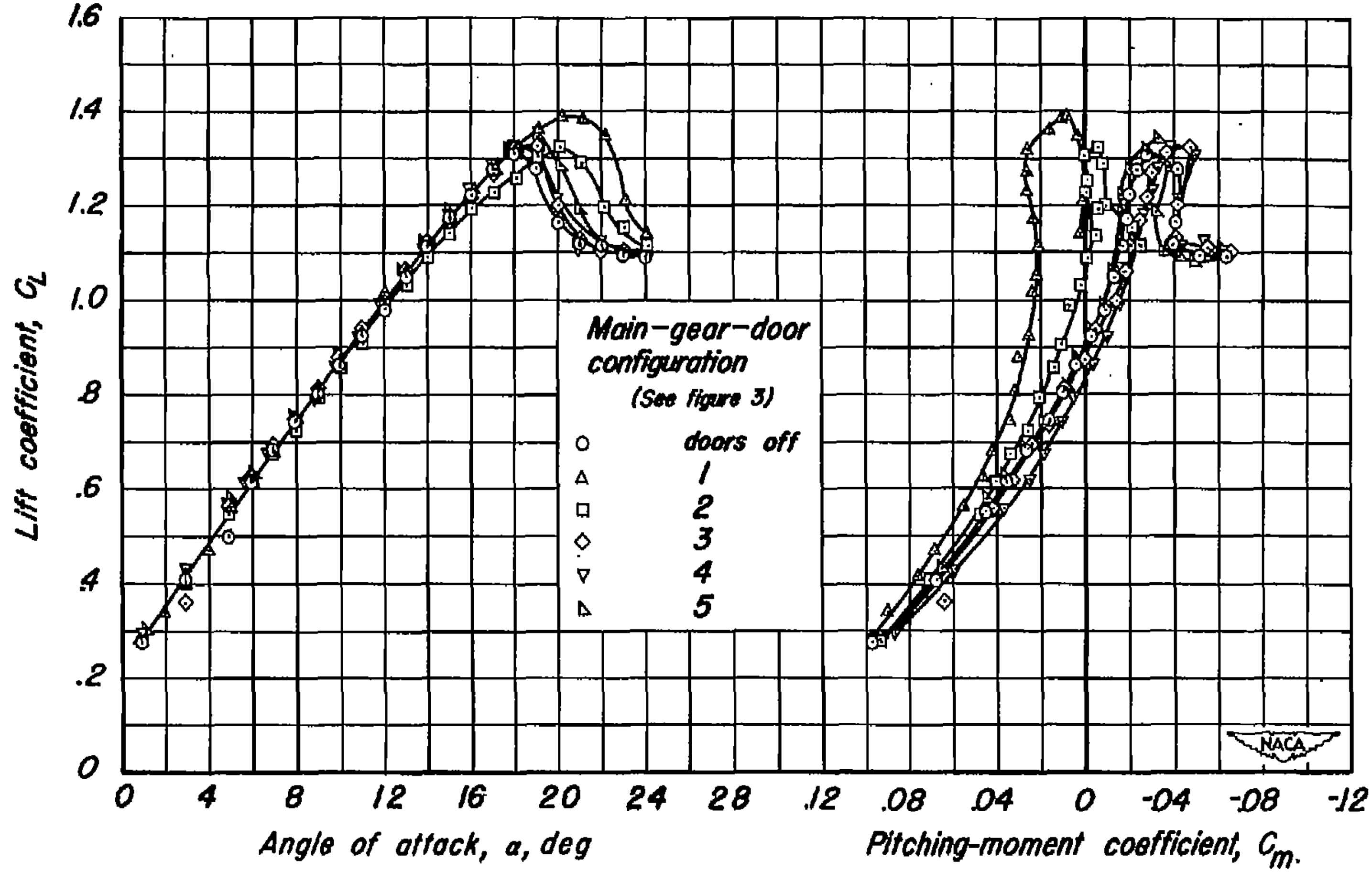

Figure 33.- The effect of various main-gear-door configurations on the longitudinal characteristics of the complete model. $\delta_{LF} = 30°$, $\delta_{TF} = 50°$; $i_t = -5°$.

[redacted]

[redacted]

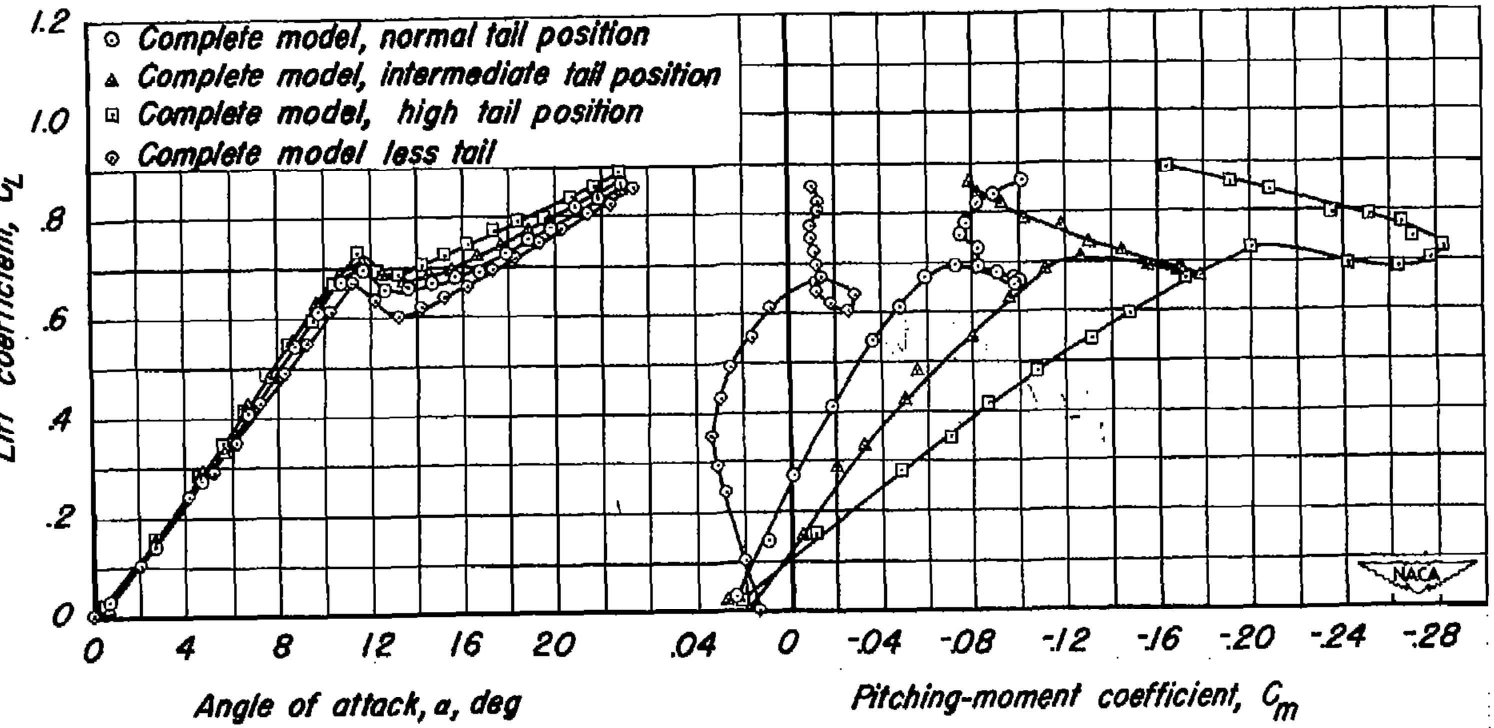

[redacted]

(a) Flaps neutral; $i_t = 0°$.

Figure 34.- The effect of the vertical location of the horizontal tail on the longitudinal characteristics of the complete model.

[redacted]

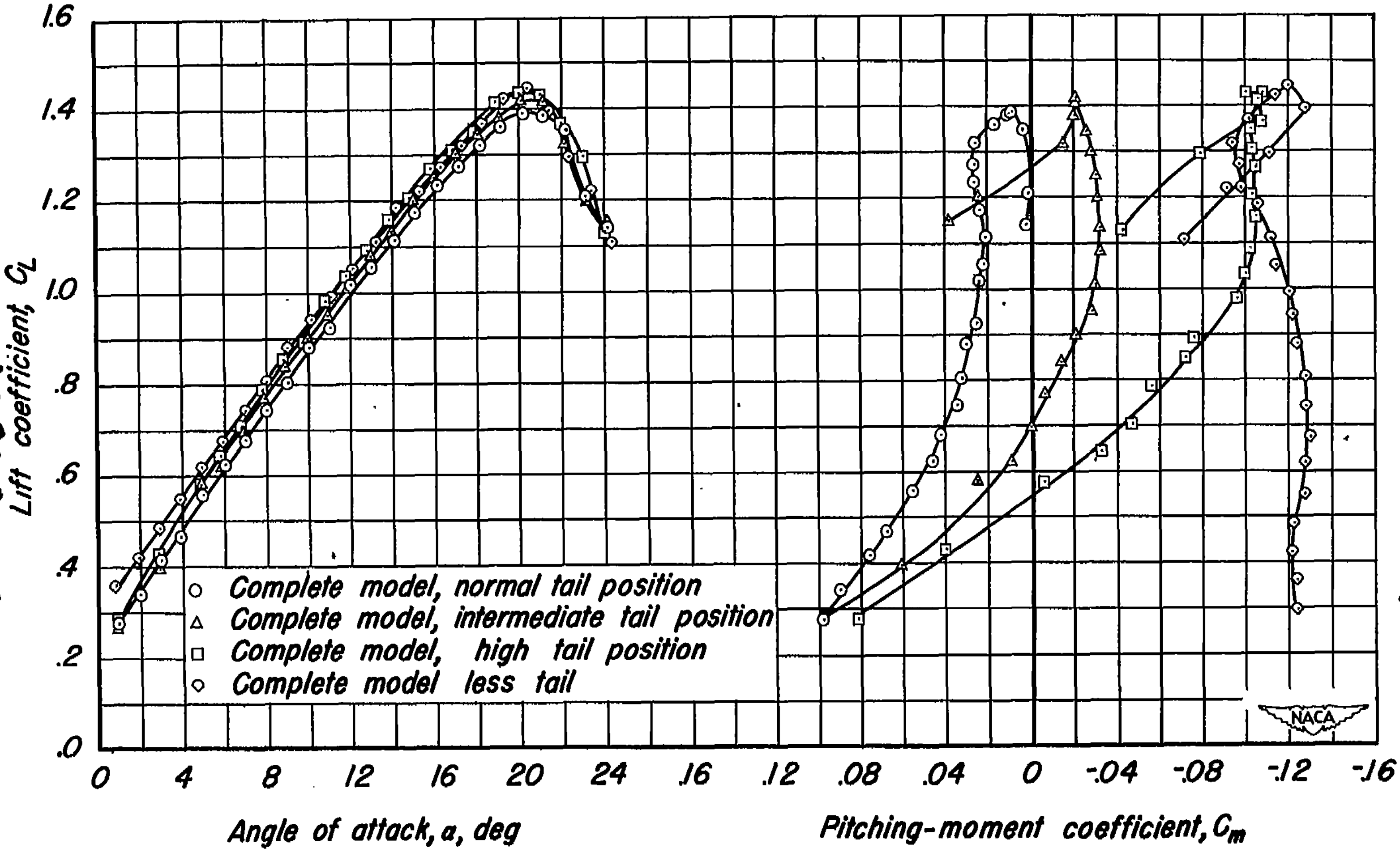

[redacted]

(b) $\delta_{LF} = 30°$, $\delta_{TF} = 50°$; $i_t = -5°$.

Figure 34.— Concluded.

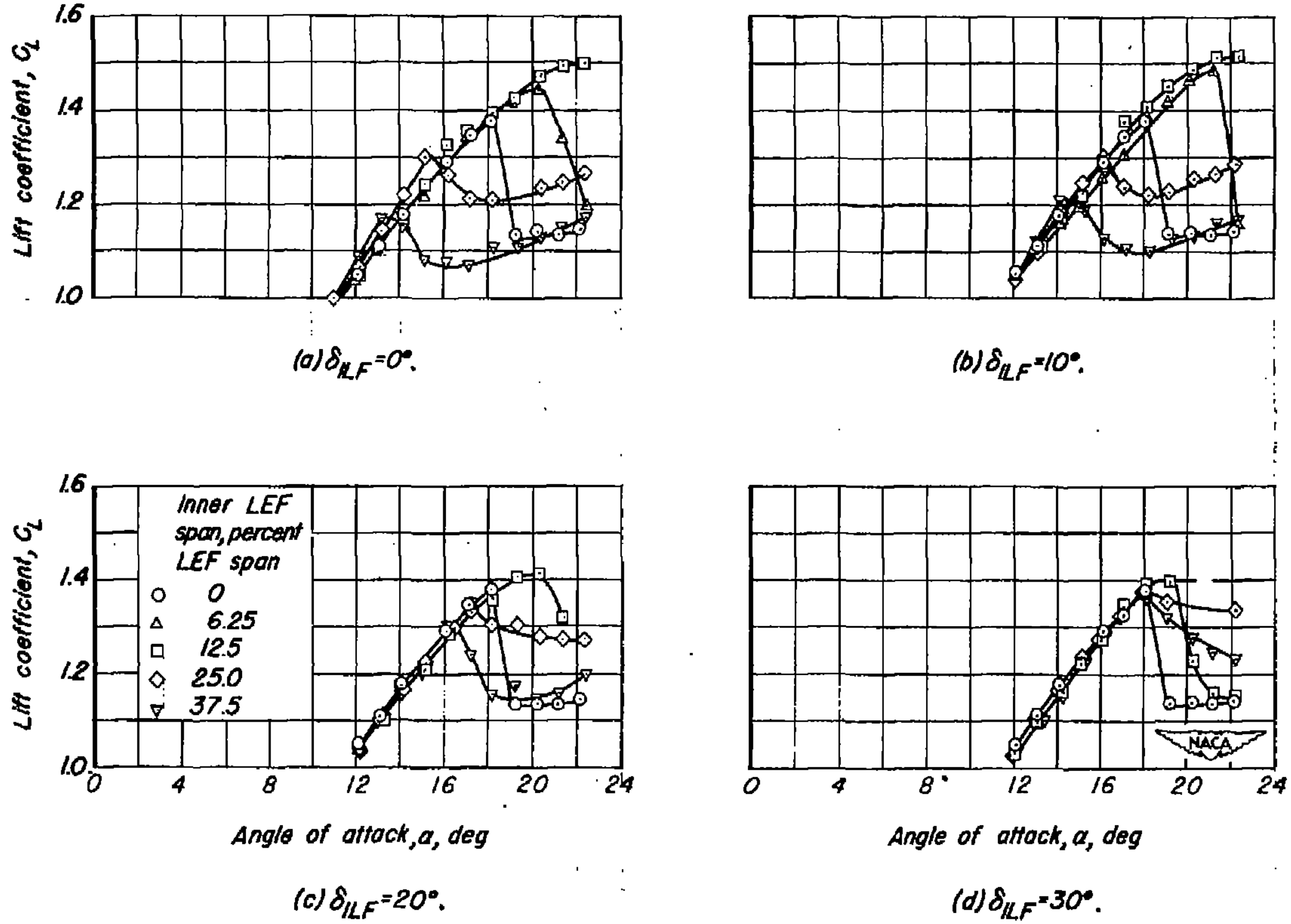

Figure 35.–The effect of the deflection and span of the inner leading-edge flap on the lift characteristics of the complete model. $\delta_{OLF}=30°$, $\delta_{TF}=50°$; $i_t=0°$.

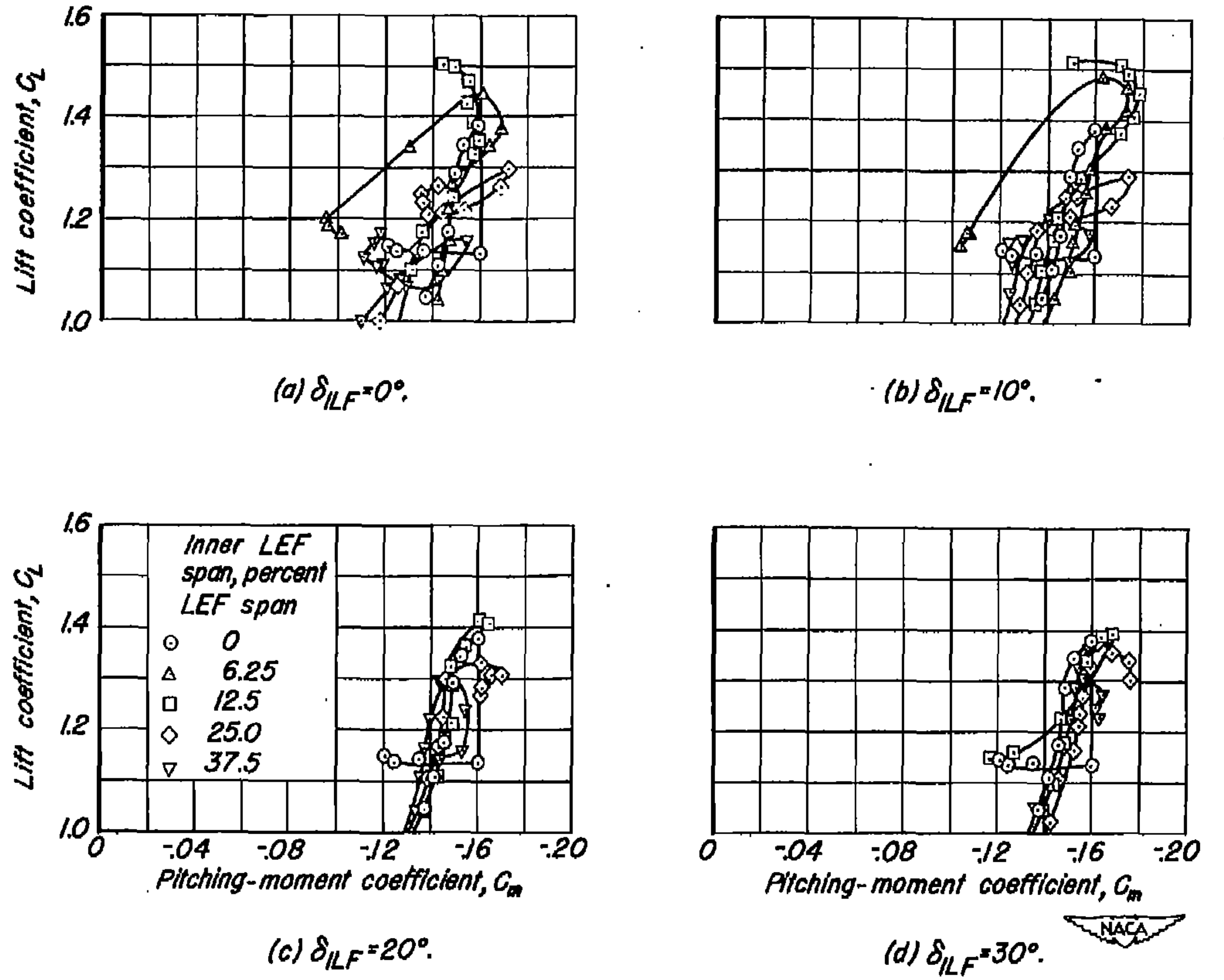

Figure 36.—The effect of the deflection and span of the inner leading-edge flap on the pitching-moment characteristics of the complete model. δ_{OLF}=30°, δ_{TF}=50°; i_t=0°.

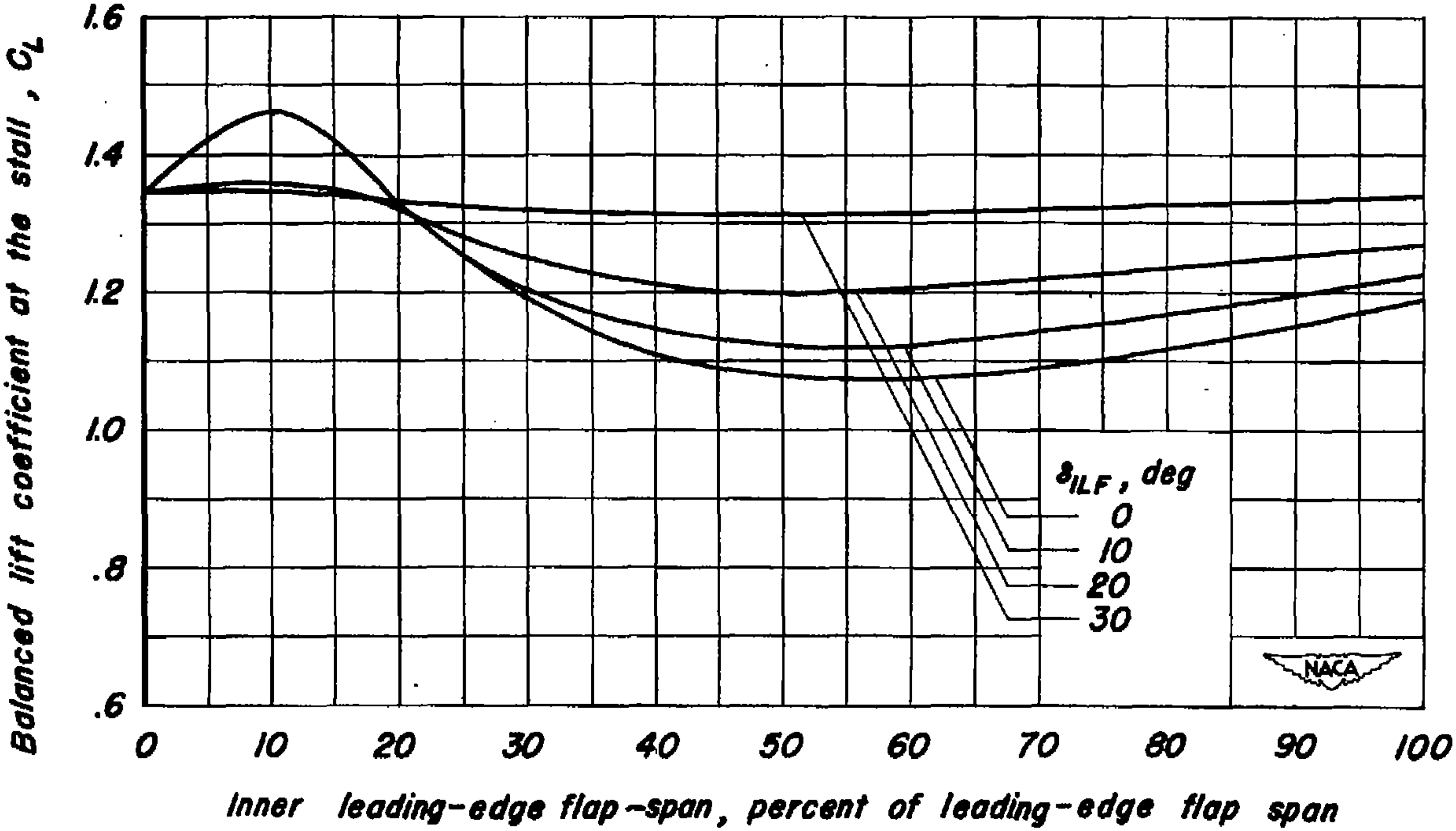

Figure 37.–The effect of the deflection and span of the inner leading-edge flap on the balanced lift coefficient at the stall of the complete model. δ_{OLF}=30°, δ_{TF}=50°.

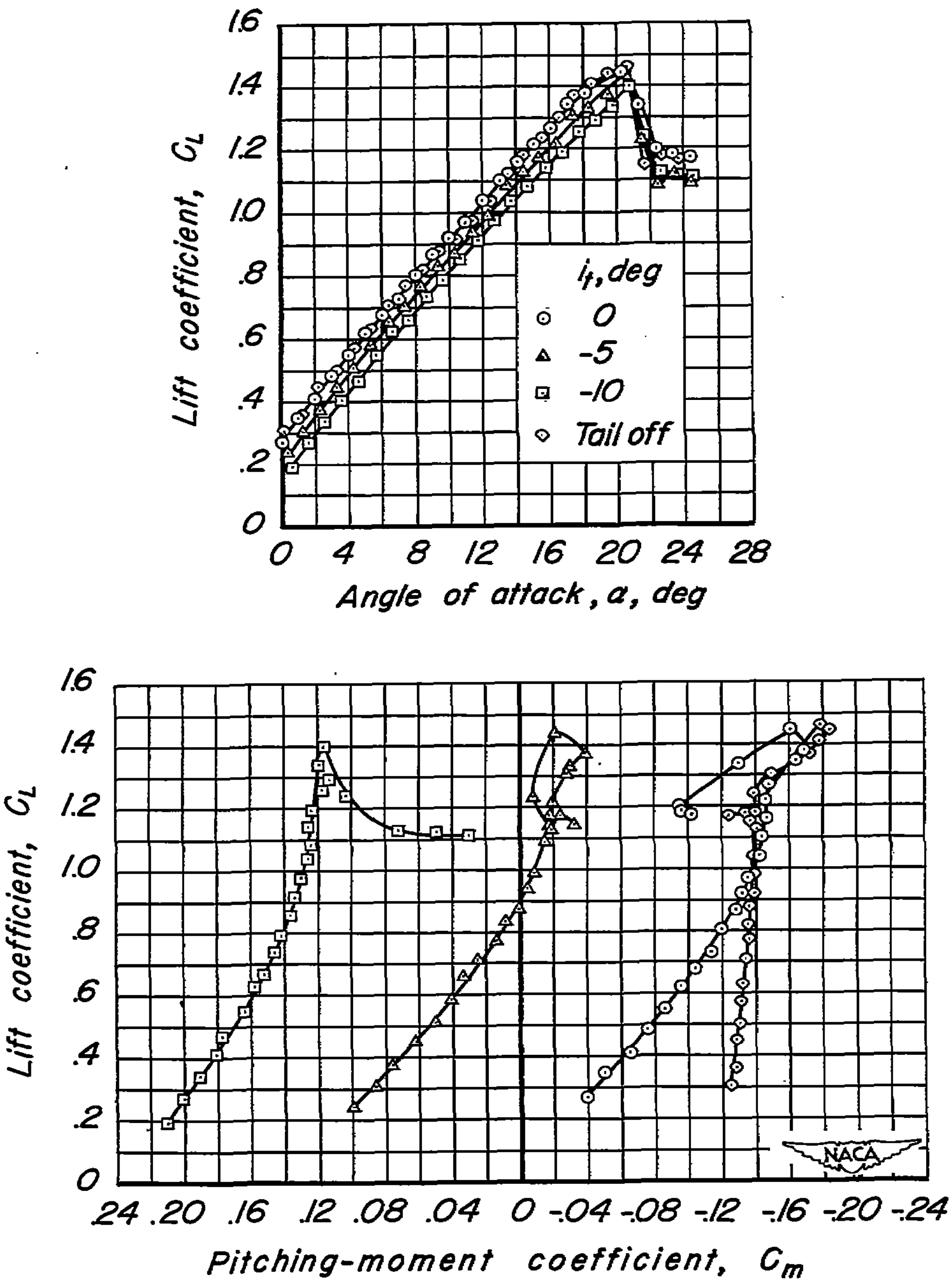

Figure 38.—The effect of the incidence of the horizontal tail on the longitudinal characteristics of the complete model with the leading-edge-flap divided at 0.0625 span. $\delta_{ILF}=0°$, $\delta_{OLF}=30°$; $\delta_{TF}=50°$.

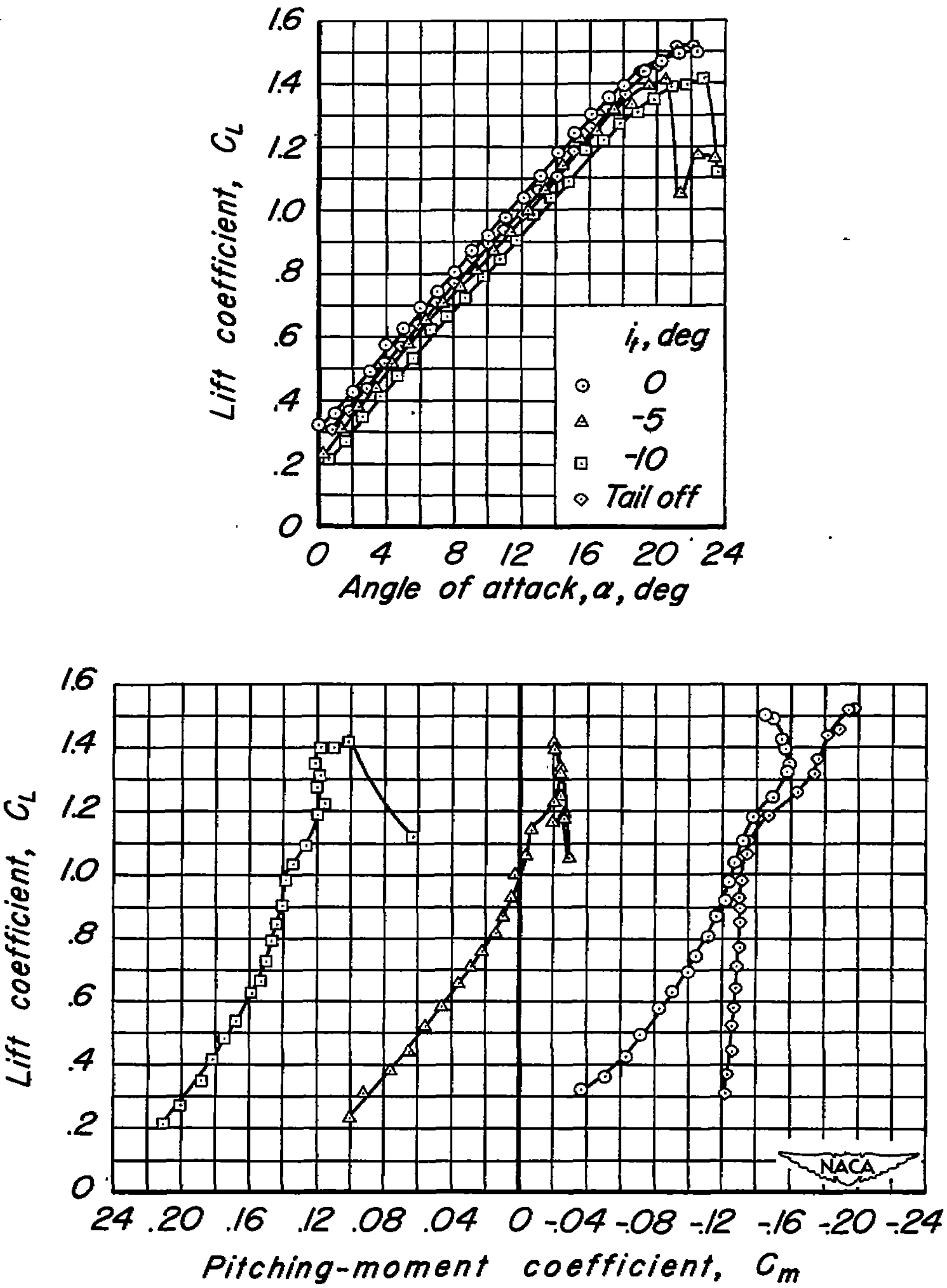

Figure 39.–The effect of the incidence of the horizontal tail on the longitudinal characteristics of the complete model with the leading-edge flap divided at 0.125 span. $\delta_{ILF}=0°$; $\delta_{OLF}=30°$; $\delta_{TF}=50°$.

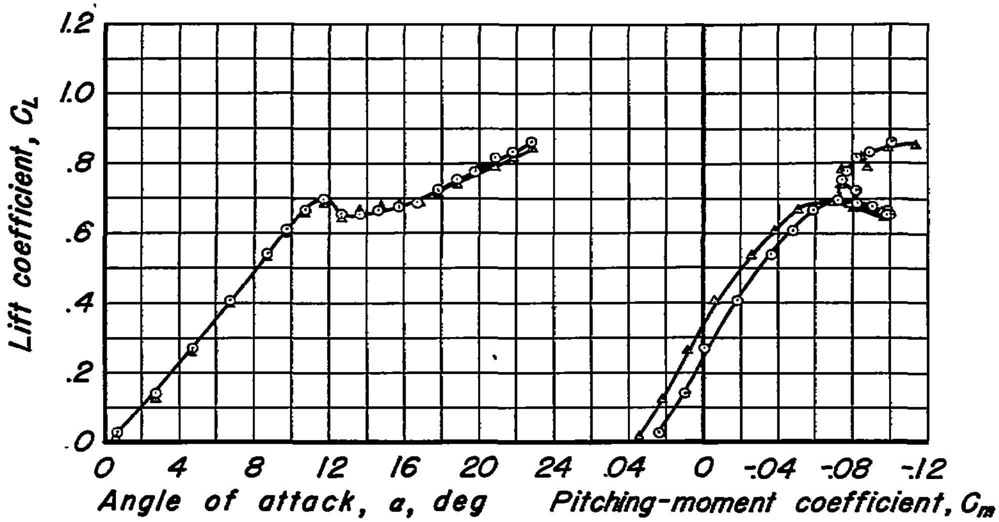

(a) Flaps neutral; $i_t = 0°$

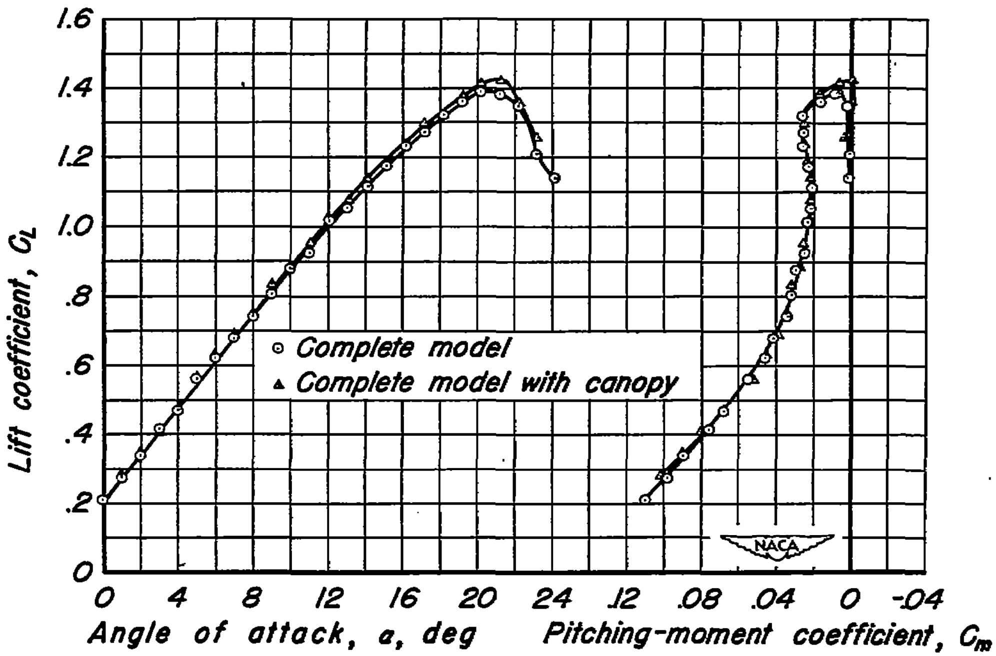

(b) $\delta_{LF} = 30°$, $\delta_{TF} = 50°$; $i_t = -5°$;
gear down with main-gear-door configuration I.

Figure 40.–The effect of the canopy on the longitudinal characteristics of the complete model.

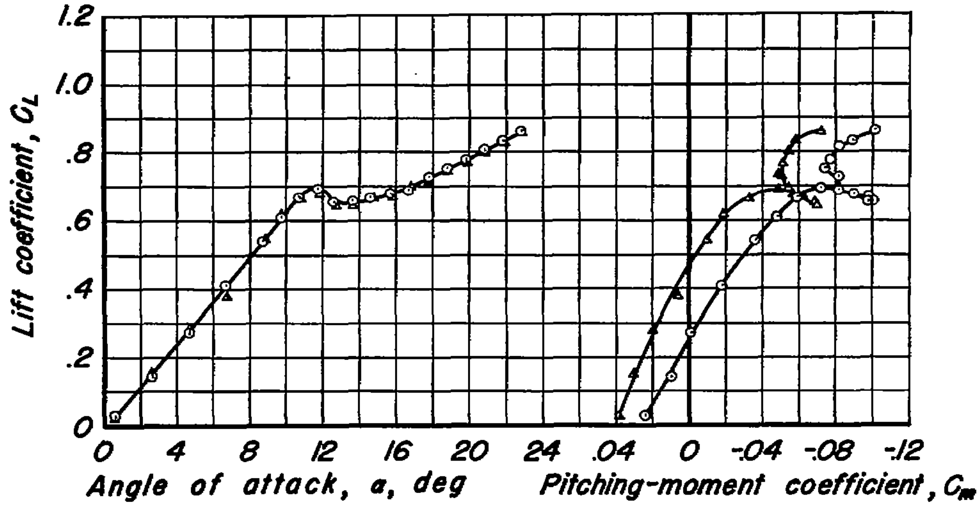

(a) Flaps neutral; $i_t = 0°$

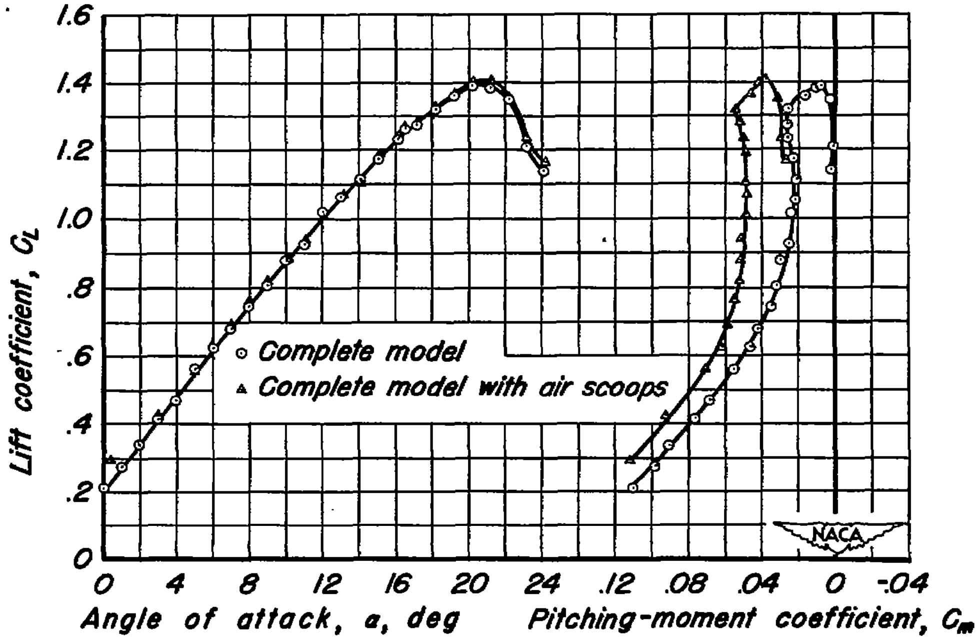

(b) $\delta_{LF} = 30°$, $\delta_{TF} = 50°$; $i_t = -5°$; gear down with main-gear-door configuration I.

Figure 41.–The effect of the air scoops on the longitudinal characteristics of the complete model.

NACA-Langley - 9-8-50 - 115